Upper Norian conodonts from the Baoshan block, western Yunnan, southwestern China, and implications for conodont turnover

Weiping Zeng [1, 2], **Haishui Jiang** [Corresp., 2], **Yan Chen** [2], **James Ogg** [2, 3], **Muhui Zhang** [2], **Hanxinshuo Dong** [2]

[1] School of Geography and Tourism, Huanggang Normal University, Huanggang, Hubei, P.R. China

[2] State Key Laboratory of Biogeology and Environmental Geology, School of Earth Sciences, China University of Geosciences, Wuhan, Hubei, China

[3] Department of Earth, Atmospheric and Planetary Sciences, Purdue University, West Lafayette, United States

Corresponding Author: Haishui Jiang
Email address: jiangliuis@163.com

The Sevatian of the late Norian is one of the key intervals in biotic turnover and in changes of paleoclimate and paleoenvironments. Conodont faunas recovered from two sections of upper Norian strata of the Dashuitang and Nanshuba formations near Baoshan City in western Yunnan province provide new insights into the diversity and biostratigraphy of the Sevatian conodonts within China as well as globally. A lower *Mockina* (*M.*) *bidentata* Zone and an upper *Parvigondolella* (*P.*) *andrusovi* Zone are identified in this area according to the first occurrences of *M. bidentata* and of *P. andrusovi*. Rich conodont fauna of *M. zapfei* is detailed and presents various intraspecific forms. A total of 19 different forms of P_1 elements are presented, which, when combined with the reported conodonts in the *M. bidentata* Zone, suggest that there was a peak in conodont diversification within the *M. bidentata* Zone. A biotic crisis in the uppermost *M. bidentata* Zone is recognized from the contrast between the diverse conodont fauna in the *M. bidentata* Zone and the barren conodonts in the *P. andrusovi* Zone. The conodont turnover during the middle Sevatian highlights the fact that the prolonged phases of the end-Triassic mass extinction probably began in the transition interval from *M. bidentata* Zone to *P. andrusovi* Zone.

Upper Norian conodonts from the Baoshan block, western Yunnan, southwestern China, and implications for conodont turnover

Weiping Zeng[1, 2], Haishui Jiang[2], Yan Chen[2], James G. Ogg[2, 3], Muhui Zhang[2], Hanxinshuo Dong[2]

[1]School of Geography and Tourism, Huanggang Normal University, Huanggang, Hubei, P.R. China
[2]State Key Laboratory of Biogeology and Environmental Geology, School of Earth Sciences, China University of Geosciences, Wuhan, Hubei, P.R. China
[3]Department of Earth, Atmospheric and Planetary Sciences, Purdue University, West Lafayette, IN, 47907-2051, USA

Corresponding Author:
Haishui Jiang[2] Lumo Road 388#, Hongshan District, Wuhan, Hubei, 430074, P.R. China
Email address: jiangliuis@163.com

Abstract

The Sevatian of the late Norian is one of the key intervals in biotic turnover and in changes of paleoclimate and paleoenvironments. Conodont faunas recovered from two sections of upper Norian strata of the Dashuitang and Nanshuba formations near Baoshan City in western Yunnan province provide new insights into the diversity and biostratigraphy of the Sevatian conodonts within China as well as globally. A lower *Mockina* (*M.*) *bidentata* Zone and an upper *Parvigondolella* (*P.*) *andrusovi* Zone are identified in this area according to the first occurrences of *M. bidentata* and of *P. andrusovi*. Rich conodont fauna of *M. zapfei* is detailed and presents various intraspecific forms. A total of 19 different forms of P_1 elements are presented, which, when combined with the reported conodonts in the *M. bidentata* Zone, suggest that there was a peak in conodont diversification within the *M. bidentata* Zone. A biotic crisis in the uppermost *M. bidentata* Zone is recognized from the contrast between the diverse conodont fauna in the *M. bidentata* Zone and the barren conodonts in the *P. andrusovi* Zone. The conodont turnover during the middle Sevatian highlights the fact that the prolonged phases of the end-Triassic mass extinction probably began in the transition interval from *M. bidentata* Zone to *P. andrusovi* Zone.

Introduction

There is growing evidence that the end-Triassic mass extinction episode was a prolonged interval comprised of multiple waves of extinctions (Benton, 1986, 1993; Bambach et al., 2004; Tanner et al., 2004; Ward et al., 2004; Lucas & Tanner, 2008; Onoue et al., 2016, 2017; Rigo et al., 2020; Wignall and Atkinson, 2020; Racki & Lucas, 2020; Lucas, 2021). This protracted Late Triassic extinction episode probably begin as early as the middle or late Norian (Sephton et al.,

2002; Tanner et al., 2004; Lucas & Tanner, 2015; Rigo et al., 2020). For example, the global diversity of marine and terrestrial tetrapods peaked during the late Carnian, then dropped steadily from early Norian through late Rhaetian to reach a nadir at the end of the Triassic (Benson et al., 2009; Benton et al., 2013). Almost all monotid bivalves disappeared around the Norian-Rhaetian boundary (Wignall et al., 2007), and significant turnovers in ammonoid and conodont faunas occurred during the late Norian (McRoberts et al., 2008) and during the Norian-Rhaetian boundary interval (Ward et al., 2001). According to the compilation of Benton (1993), seven families of gastropods had gone extinct by the end of the Norian, whereas none underwent an extinction during the end-Triassic and 35 families continued into the Jurassic. Onoue et al. (2016) concluded that a succession of radiolarian extinctions took place at the mid-Norian, the Norian-Rhaetian boundary interval and the Triassic-Jurassic boundary. Rigo et al. (2020) placed the onset of the prolonged set of Late Triassic mass extinctions as at or very close to the Norian/Rhaetian boundary based on $\delta^{13}C_{org}$ data from sections distributed around the world. Other evidence suggests that the onset was slightly earlier during the Sevatian.

During the Sevatian of the Late Norian, many genera underwent significant turnover events or extinctions and there were significant changes in paleoclimate and paleoenvironments. McRoberts (2010) observed that almost all of the bivalves of the *Halobia* and *Eomonotis* genera disappeared and those of *Monotis* began to appear during the Alaunian/Sevatian transition (ca. 217~213 Ma). Baranyi et al. (2018) quantitatively analyzed the pollen data of the Chinle Formation in the southwestern United States and found that turnovers in plants also occurred during this Alaunian/Sevatian transition, in addition to other significant changes in flora and fauna in the middle of the Chinle Formation. Qualitative and quantitative analysis of sporopollen in Poland documented a shift to hygrophytes during the Sevatian, indicating a small change to more humid climates (Mader, 2015). Benton et al. (1986) proposed that diversity of genera of ammonoids declined sharply during the Late Norian. Wiedmann and Kullman (1996) further pointed out about 14 genera disappeared at the Alaunian/ Sevatian boundary followed by a further progressive or, at least gradual, decline in diversity of ammonoids during the Sevatian through Rhaetian. Lucas (2018) summarized previous studies on ammonoids and suggested that, as the diversity of ammonoids decreased, heteromorphs appeared during the Sevatian. Onoue et al. (2016, 2017) observed a gradual extinction of radiolarians in the "*Epigondolella*" (=*Mockina*) *bidentata* Zone of the Sevatian substage in the Sakahogi section of Panthalassa, and a short negative shift of $^{187}Os/^{188}Os$ and $\delta^{13}C_{org}$ values in the lower *Mockina bidentata* Zone. In contrast, calcareous ultra-microplankton expanded and diversified in the *Mockina bidentata* Zone of the Sevatian (Gardin et al., 2012； Preto et al., 2013; Demangel et al., 2020).

In terms of the climatic and environmental trends, the curve of $^{18}O_{phosphate}$ from Triassic conodonts shows a prominent negative shift in the lower Sevatian, which indicates an interval ("W3") of relatively warm and humid climate (Trotter et al., 2015), even though proxies from paleosol carbonate rocks in the Newark and Hartford basins of the United States suggest a significant decrease in atmospheric pCO_2 concentration during the Sevatian (Schaller et al., 2015; Kent et al., 2017). Zaffani et al. (2017) identified three negatively biased events (S1, S2 and S3) by the Sevatian portion of the $\delta^{13}C_{org}$ curves of the Pignola-Abriola, the Mt Volturino and the Madonna del Sirino sections in southern Italy, which enhanced the broader negative shift in $\delta^{13}C_{carb}$ recorded by Muttoni et al. (2014). There was a rapid northward dispersal of sauropods from Gondwana to temperate Europe and Greenland (215-212 Ma, Kent & Clemmensen, 2021). The Manicouagan impact event (215-214 Ma, van Soest et al., 2011; Sato et al., 2021) in Canada might have punctuated these climatic trends.

Therefore, the Sevatian substage of the Norian is one of the key intervals in biological evolution within the Late Triassic and heralds the onset of the series of end-Triassic mass extinctions. The major changes in biology and climate occurred during the conodont *M. bidentata* Zone or in the transition interval of *M. bidentata* Zone/*P. andrusovi* zone. Conodonts, prior to their total extinction in the latest Triassic, have advantages in the study of the biotic events and reconstruction of precise biostratigraphy during the Triassic because of their rapid evolution, wide distribution and well-preserved characteristics. Nevertheless, conodonts of the Sevatian have been poorly studied; indeed, current research records suggest an anomalously low rate of conodont evolution during the Sevatian (Orchard, 2018; Rigo et al., 2018). In particular, it appears that the duration of the single *M. bidentata* Zone was more than 5 Myr, which is inconsistent with the typical fast-evolving nature of these conodont animals. However, evolving and disputed concepts of the classification and identification of conodonts of Sevatian age might have distorted this picture.

Development and complexity of Sevatian conodont biostratigraphy

Huckriede (1958) established a vaguely defined form species of "*Polygnathus*" *abneptis,* which contains various denticulated P_1 elements, and some of these denticulated specimens occurred in the Sevatian substage of the Mediterranean. Mosher (1968) established *M. bidentata* and summarized that "*Epigondolella* (*E.*)" *abneptis* and *Norigondolella* (*N.*) *steinbergensis* co-occurred with *M. bidentata* in Europe, whereas only "*E.*" *abneptis* occurred in the *M. bidentata* Zone in North America. However, because the original definition of "*E.*" *abneptis* was based on a variety of platform conodonts (Huckriede, 1958; Karádi, 2018), "*E.*" *abneptis* actually includes many different forms of P_1 elements, which indicates a more diverse suite of conodont fauna in *M. bidentata* Zone. Kozur & Mostler (1972, table 1) suspected that *M. postera* may range into the Sevatian of the Tethyan Triassic strata of Europe (excluding the Far Mediterranean Basin and Greece). Kovács & Kozur (1980, table 2) presented stratigraphic ranges for the most important Middle and Upper Triassic conodonts, and indicated that *M. mosheri*, *N. steinbergensis, M. postera*, *M. longidentata* and *O*? *multidentata* occurred in *M. bidentata* Zone. Krystyn (1980, figs. 6, 8) also complied that *M. postera*, "*E.*" *abneptis* and *N. steinbergensis* range into *M. bidentata* Zone. The taxa of *M. postera* (Wang & Dong, 1985; Gullo, 1996; Channell et al., 2003; Muttoni et al., 2004; Rožič et al., 2009) and *N. steinbergensis* (Channell et al., 2003; Hornung, 2005; Rožič et al., 2009; Mazza et al., 2012; Onoue et al., 2018; Du et al., 2020) are reported in many places in the Tethyan realm. Wang & Dong (1985) first presented eastern Tethyan platform conodonts of Norian age in Baoshan area, Yunnan Province of China, and showed that *M. postera*, "*E.*" *abneptis spatulatus*, "*E*" *multidentata* and "*E.*" *abneptis abneptis* are associated with *M. bidentata*.

Many other form species accompanying *M. bidentata* in the Tethys realm have been discovered during the 21st century. *M. zapfei* (Channell et al., 2003; Giordano t al., 2010; Rigo et al., 2018; Du et al., 2021; Jin et al., 2022), *M. slovakensis* (Gullo, 1996; Giordano et al., 2010; Muttoni et al., 2004; Rigo et al., 2018; Du et al., 2021; Jin et al., 2022) and "*P.*" *vrielyncki* (Channell et al., 2003; Rigo et al., 2018; Du et al., 2021) are common species that occur in the *M. bidentata* Zone. "*M.*" *englandi* (Krystyn et al., 2007; Onoue et al., 2018; Du et al., 2020) and "*M.*" *carinata* (Du et al., 2020) are also reported. Karádi (2021) displayed "*Orchardella*" *mosheri* morphotype B and *M. englandi* from Hungary, but did not state whether the P_1 elements of the two form species were found in the *M. bidentata* Zone. Some different forms of P_1

elements identified as *M. mosheri* morphotype B or morphotype A (Du et al., 2020, fig. 3.8; Krystyn et al., 2007, pl. 1, fig. 6; Jin et al., 2022, fig. 4.8) occur in the *M. bidentata* Zone. Segminate P_1 elements of *P. lata* (Du et al., 2021), conical P_1 elements of *Zieglericonus* (Channell et al., 2003; Du et al., 2021) and transitional forms with just one marginal denticle and no or extremely reduced platform are found in the *M. bidentata* Zone (Karádi et al., 2020; Du et al., 2021; Zeng et al., 2021). In addition, many undefined species or forms of P_1 elements are documented in the *M. bidentata* Zone, such as *M*. cf. *zapfei* (Channell et al., 2003), *M. carinata*? (Du et al. 2020, fig. 3.9), *M*. cf. *slovakensis* (Channell et al., 2003), *E. triangularis*? (Channell et al., 2003), *Mockina* sp. (Du et al., 2020), *M*. aff. *tozeri* (Mazza et al., 2012; Onoue et al., 2018), *E*. *uniformis*? (Mazza et al., 2012; Onoue et al., 2018), etc. Zeng et al. (2021, fig. 2.3) first found *M. sakurae* and Jin et al. (2022) erected a new species *M. passerii* Rigo and Du, 2022 in the *M. bidentata* Zone of the Baoshan area, China.

In North America, there are only a few reported association form species in the *M. bidentata* Zone; mainly these are *E. englandi* (Krystyn et al., 2007; Onoue et al., 2018; Du et al., 2020), *E. carinata* (Du et al., 2020), *N. steinbergensis* and unidentified species of *Parvigondolella* (Orchard, 1991b; Orchard et al., 2007b). In Japan of the Panthalassa realm, Yamashita et al. (2018) figured eight different forms of P_1 elements from the *M. bidentata* Zone, and respectively assigned these to *M. spiculata*, *M. elongata*, *M. mosheri* A, *M. slovakensis*, *Mockina* sp. indet. A, *Mockina* sp. indet. B and *P*. aff. *vrielyncki*.

The overlying *P. andrusovi* Zone was first introduced by Kovács and Kozur (1980), who put it above the *M. bidentata* Zone and below the *Mi. hernsteini* Zone and with an interpreted age corresponding to the middle of the ammonoid *Cochloceras suessi* Zone. Gaździcki et al. (1979) used these three conodont biozones to subdivide Sevatian strata of the Alpine-Mediterranean Triassic. Later, Kozur (2003), Channell et al. (2003), Rožič et al. (2009) and Gale et al. (2012) combined the *P. andrusovi* and *Mi. hernsteini* into one single biozone. At present, *P. andrusovi* Zone is widely recognized in the Tethyan realm (Rigo et al., 2018; Karádi et al., 2020; Du et al., 2021; Zeng et al., 2021). Yamashita et al. (2018) discovered *P. andrusovi* in Japan. In North America, despite no *P. andrusovi* having been reported, several species of *Parvigondolella* occur from the upper Norian to the Rhaetian (Carter & Orchard; Orchard et al., 2007a, b).

This overview indicates that conodont form species are more abundant and varied in the *M. bidentata* Zone of the early Sevatian than initially thought, and that more detailed research of the fauna is required in order to enhance the database for conodont biostratigraphy, evolution and diversity. It is essential that such studies include a more precise intercalibration to other biostratigraphic, geochemical and magnetostratigraphic scales. China, located in the eastern Tethys, has Sevatian strata distributed in Heilongjiang of northeastern China (Table 1, Wang et al., 1986; Wang & Wang, 2016), Tibet of southwestern China (Table 1, Mao & Tian, 1987; Yi et al., 2003; Ji et al., 2003) and Western Yunnan of southwestern China (Table 1, Wang & Dong, 1985; Dong & Wang, 2006; Du et al., 2020; Zeng et al., 2021; Jin et al., 2022). However, the investigation on Norian conodonts in these locations is very limited and many conodont taxa are not updated (Table 1). For example, the presented specimens identified as "*E*." *multidentata* in the documentations given in Table 1 actually all have different morphological features from *O*? *multidentata*. For example, the specimen (Wang & Dong, 1985, pl. 1, fig. 16) identified as "*E*." *multidentata* has three and one marginal denticles, respectively, on each anterior platform margin, which more resembles *M. zapfei* (see entry below in Systematic paleontology), and the other specimen of "*E*." *multidentata* (Wang & Dong, 1985, pl. 1, fig. 17) differs from *O*? *multidentata* by having only one inner anterior marginal denticle and denticulated posterior

platform margins. As our paper mainly focuses on the conodont diversity during the Norian, especially the Sevatian, we don't discuss the accuracy of conodont classification and hence retain the authors' original taxonomy in Table 1.

Only a few studies have focused on the late Norian conodonts of the Baoshan area. The first by Wang and Dong (1985) established an "*E." postera* Zone and "*E." bidentata* Zone, and assigned most of the Dashuitang Formation to their "*E." postera* Zone and the upper Dashuitang Formation and the lower Nanshuba Formation to their "*E." bidentata* Zone. Even though the P_1 elements illustrated in Wang and Dong (1985) only present a single view, at least 8 different forms in upper view can be discerned. Late, Wang et al. (2019) discovered "*M." englandi* (Orchard, 1991b), "*M.*" aff. *englandi* and *M. bidentata* in the Dashuitang Formation. Du et al. (2020) presented several additional forms of Norian conodonts from the Nanshuba Formation. Zeng et al. (2021) illustrated *M. sakurae* (fig. 2.3), *P. andrusovi* (figs. 1/e, 4/3), P_1 elements with only one marginal denticle and no platform (figs. 5.2h, 5.7) and P_1 elements with only a pair of anterior marginal denticles and squared, smooth posterior platform (fig. 4.2b-d) for the first time from the Baoshan area. Jin et al. (2022) first reported *M. slovakensis* from the Baoshan area and erected *M. passerii* Rigo and Du, 2022. These studies imply that the conodonts in the Upper Triassic strata of the Baoshan block are probably very diverse.

Therefore, because the Baoshan area of western Yunnan has yielded relatively diverse late Norian conodonts (Wang & Dong, 1985; Du et al., 2020; Zeng et al., 2021; Jin et al., 2022) and has easy access, we performed a detailed study of conodonts in two sections in Baoshan to acquire a detailed set of data to gain a better understanding of the Sevatian conodonts of eastern Tethys.

Geological setting

The conodonts described in this paper were recovered from the Madoupo section (MDP) and the Potou section (POT), which are located about 5 to 6 km apart in the Longyang district, Baoshan city, western Yunnan Province, southwestern China (Fig. 1C). These two sections are situated in the Baoshan tectonic block, which is the current northern part of the Sibumasu terrane (Fig. 1A, Ali et al., 2013; Liao et al., 2015; Cai et al., 2017) and may have accreted to South China during the Late Triassic or Early Jurassic (Sone & Metcalfe, 2008; Morley, 2018). The upper Triassic marine sediments of the Baoshan block are well developed (Figs. 1A, 1B), and can be subdivided into the Dashuitang Formation and the Nanshuba Formation (Li, 1976; BGMRY, 1980, 1981; Wang & Dong, 1985; Zhao et al., 2012; Wang et al., 2019; Du et al., 2020; Jin et al., 2022). The ages of the outcropping limestones of the Dashuitang Formation and of the Nanshuba Formation are constrained by conodonts and radiolarians as Alaunian-Sevatian and as Sevatian respectively (Wang & Dong, 1985; Wang et al., 2019; Du et al., 2020; Jin et al., 2022).

The interpretations of the depositional environments of the Dashuitang and Nanshuba formations are inconclusive. The earliest studies inferred that the Upper Triassic strata on the Baoshan block were deposited in littoral to shallow-marine environments (Fig. 1B) (BGMRY, 1980; BGMRY, 1990). Hao et al. (1999) thought that the limestone of the Dashuitang Formation was a shallow carbonate platform facies. Bao et al. (2012) discovered seismites in the Dashuitang Formation in the Jinji area of Baoshan, and therefore concluded that it deposited in a slope-basin environment. Peng et al. (2014) found carbonate-clastic turbidites in the Dashuitang Formation at Yaoguan of western Yunnan, and inferred that it was deposited in a rifted trough basin. Wang et al. (2019) deduced from the microfacies of the upper limestone of the Dashuitang

Formation in the Dabaozi area of Baoshan that the setting was a continental shelf environment. Wu et al. (2020) subdivided the Dashuitang Formation deposits in the Hongyan section into eight microfacies, and distinguished three different depositional settings – deep-water shelf facies, slope facies, and base-of-slope facies – within a generally relatively low-energy deep-water environment, which corresponded to an extensive transgression during Late Triassic across northwestern Yunnan.

For the overlying Nanshuba Formation, most researchers agree that it was deposited in deeper waters than the Dashuitang Formation, but dispute whether the Nanshuba Formation was deposited on the marginal part of a slope-basin (Zhao et al., 2012), on the marginal part of a rifting seaway (Wang et al., 2000), or on the shelf of a shallow island arc with steep slopes (Wang et al., 2019). The Nanshuba Formation in Baoshan area is dominated by calcareous mudstone and sandy mudstone but with a few interbeds of marl and limestone. Regionally, the total thickness of this formation ranges between 800–1400 m, but varies dramatically laterally. The thickness of the interbedded limestones can be up to 100 m (BGMRY, 1990, p. 194).

The lower ca. 13 m of the Potou section is mainly composed of grayish yellow thick-bedded bioclastic limestone and greyish white medium-bedded limestone of the upper Dashuitang Formation. The exposed strata are slightly fragmented and weathered on the surface of the section. The Dashuitang Formation at the Potou section conformably underlies the Nanshuba Formation, which was not well exposed due to two significant covered intervals and with herbage and low shrubs hiding other parts. The lower part of the Nanshuba Formation exposed below the first covered interval consists of thin- to medium-bedded grey to white limestone and an upper greyish green shale interbedded with grayish-yellow marl. The upper parts of the Nanshuba Formation exposed at the Potou section mainly consist of medium-bedded greyish white bioclastic limestone and micritic limestone. The Madoupo section is relatively continuous, ca. 56-m exposure, with the lower part along a hiking road transitioning to the upper part at the top of the hill. It mainly consists of grey micritic limestone with a few beds of bioclastic limestone. The intervals of the Nanshuba Formation studied by Wang et al. (2019) and by Du et al. (2020) could be stratigraphically lower than our studied section.

Materials & Methods

Limestone samples at the Baoshan block were collected from the Madoupo section (26 samples) and the Potou section (14 samples) (for sampling positions see Fig. 2). The weight of each sample from the Potou section ranges between 5 and 10 kg. No precise weights were made of the samples from the Madoupo section, but each sample weighed no less than ~5 kg. The samples were crushed into small pieces and processed in a 10% solution of acetic acid. The process of extracting conodonts is detailed in Jiang et al. (2019) and Yuan et al. (2015).

Six samples of the Madoupo section yielded conodonts (Table 2), but only five of the samples (MDP7, MDP8, MDP10, MDP12 and MDP25) yielded identifiable P_1 elements and these show a Color Alteration Index (CAI) of 1–1.5. A total of 126 identifiable P_1 elements were obtained from the Madoupo section, most of which were collected from the sample MDP8. All samples from the Potou section yielded conodonts, and these show a CAI value of 1–2. A total of 52 identifiable P_1 elements were collected. The collected specimens were photographed using a scanning electron microscope (SEM).

Repository and institutional abbreviation —All conodonts examined in this study are deposited in the School of Earth Sciences, China University of Geosciences, Wuhan, Hubei, P.R. China.

Results

The occurrence and distribution of conodont taxa in each bed are shown in Figure 2 and Table 2. Two conodont zones are discriminated based on the first occurrences (FO) of *M. bidentata* and of *P. andrusovi*. Marker species of *M. bidentata* are distributed nearly throughout the entire Potou section. The lower part of the Madoupo section that yielded conodonts also recovered *M. bidentata*. *P. andrusovi* first occurs at the ~29.5 m level in the Potou section above the appearance of a transitional form between *M. bidentata* and *P. andrusovi* and *Parvigondolella.* sp.. Accordingly, taking the layer with the lowest occurrence of *P. andrusovi* as the zonal boundary, then the Potou section can be divided into a *M. bidentata* Zone and a *P. andrusovi* Zone. As only one specimen of a ?transitional form between *M. bidentata* and *Mi. hernsteini* was found in the uppermost part of the Madoupo section, then it is inferred that the entire Madoupo section is still within the *M. bidentata* Zone.

***Mockina bidentata* Zone** —Lower limit: the first occurrence (FO) of *M. bidentata*. Upper limit: the FO of *P. andrusovi* (Rigo et al., 2018).

Associated taxa in the Potou section: *E. carinata*, *E.* aff. *englandi*, *E. passerii*, *Epigondolella* sp., *Mockina* sp., *Norigondolella*? sp. indet., *Parvigondolella* sp., *P.*? *vrielyncki*, *Zieglericonus*? sp. and transitional form between *M. bidentata* and *P. andrusovi*. A total of ten different forms of P_1 elements occurred in *M. bidentata* Zone. One broken specimen presents characterizations of genus *Norigondolella* (Fig. 3PP–3QQ), with flat and unornamented platform margins which extend to or near the anterior end and may have intense microcrenulation, with an excavated groove and with laterally compressed denticles which are fused in the lower parts and are separated near the tips. Five P_1 elements has only one marginal denticle and no platform, which were also presented in the *P. andrusovi* Zone of the Xiquelin section in Baoshan area (Zeng et al., 2021). Karádi et al. (2020) and Du et al. (2021) illustrated in detail that this form of P_1 elements is a transitional form between *M. bidentata* and *P. andrusovi.*

Associated taxa in the Madoupo section: ?*Ancyrogondolella* (*A.*) *praeslovakensis*, *E. carinata*, *E.* aff. *englandi*, *E. passerii*, *Epigondolella* sp., *M. elongata*, *M. medionorica*, ?*M. medionorica*, *M. zapfei*, *Mockina* sp. A, *Zieglericonus*? sp. and a probable transitional form between *M. bidentata* and *Mi. hernsteini.* A total of 12 different forms of P_1 elements.

One broken P_1 element has sub-symmetrically bifurcated keel end, denticulated anterior platform, smooth posterior platform margins, anterior-located cusp, submedian pit, highly fused blade denticles, abrupt blade end and peculiar arched lateral profile of the base (Fig. 3MM–3OO), which are identical with *A. praeslovakensis*. However, the classification of this P_1 element can't be totally confirmed due to the broken posterior platform. *M. medionorica* previously was commonly recovered from the Alaunian of the western Tethys (Kovács & Kozur, 1980; Vrielynck, 1987; Kozur, 2003; Channell et al., 2003; Karádi et al., 2021) and of the Panthalassa (Ishida & Hirsch, 2001), its occurrence in the lower Sevatian of the Madoupo section in eastern Tethys indicates that it has a long range and wider distribution.

Both sections yield *E. carinata, E.* aff. *englandi*, *E. passerii and Epigondolella* sp.. One conic element from the Madoupo section bears a small node above the anterior base (Fig. 4T–

4U), the other conic element from the Potou section possesses a small node above the posterior base (Fig. 4V–4W), and both conic elements have a normally expanded and moderately excavated basal cavity; and these features are apparently different from the morphological characteristics of the existing species of *Zieglericonus* which has only one conical cusp, widely expanded and deeply excavated base. It is easy to confuse the two conic elements with some broken ramiform elements of multi-element apparatuses. Many studies show that the groove or basal cavity extends from either side of the pit under the cusp in S_0, S_2, S_{3-4}, and M elements of a multi-element apparatus (Goudmand et al., 2011, 2012; Orchard, 2005; Zhang et al., 2017; Demo, 2017; Huang et al., 2018a, b; Zeng et al., 2021), which means that if the four types of ramiform elements broke around the cusp, there should be fracture marks on both ends of the basal groove. However, the well-preserved anterior end of the basal cavity in both conic elements from the Potou section and the Madoupo section shows no interruption, and hence can't be the broken S_0, S_2, S_{3-4}, and M elements. The two conic elements also can't be broken grodelliform S_1 elements as there is no additional node develops before the terminal cusp or the denticle (commonly there are 2 denticles) after the terminal cusp is long. In view of the small sample size, the two conic elements are temporarily classified as ?*Zieglericonus* sp..

Mockina medionorica (Figs. 5Y–5BB), which has previously been reported only in the Alaunian of the middle Norian, was discovered by us in the Sevatian strata. The occurrence of *M. medionorica* and *M. elongata* (Figs. 5A–5X) in the *M. bidentata* Zone may indicate that many conodont species considered as middle Norian survived into the late Norian.

Transitional forms from *M. bidentata* occur in the Potou section. Large *M. bidentata* with long blades occur from levels 14 to 19 m in the Potou section (from POT4 to POT8), below the interval with small transitional forms with no more than six denticles (Figs. 6VV–6AAA) and above the interval having large transitional forms with more than seven denticles (Figs. 6PP–6QQ, 6RR–6SS). Therefore, above the sampling layer of POT8 in the Potou section, the entire evolutionary line from the large *M. bidentata* to *P. andrusovi* is present in stratigraphic order, which is *M. bidentata* –> transitional form between *M. bidentata* and *P. andrusovi* –> *Parvigondolella* sp. –> *P. andrusovi* (shown by the white arrows in Fig. 6). Therefore, it can be inferred that the age of the Potou section ranges from the upper *M. bidentata* Zone to the lower *P. andrusovi* Zone. The transitional form of P_1 elements with only one marginal denticle is also productive in the *P. andrusovi* Zone of the Xiquelin section in the same area (Zeng et al., 2021, figs. 5.2h, 5.7), thereby indicating a wide distribution in the Sevatian of the Baoshan block.

Another transitional P_1 element from *M. bidentata* recovered from the Madoupo section (Fig. 6BBB–6CCC) differs from the transitional form between *M. bidentata* and *P. andrusovi* by the terminal big cusp and the moderately opened and excavated posterior base. *P. lata*, *P. ciarapicae* and *Mi. hernsteini* all have big terminal cusps, but the posterior base or keel (commonly posterior to the pit) of *P. lata* and *P. ciarapicae* is commonly not excavated and hence the pit can be easily discerned. The posterior basal cavity of this P_1 element resembles that of *Mi. hernsteini*, therefore it seems that the P_1 element can evolve into *Mi. hernsteini* by further opening the groove anterior to the pit and missing the marginal denticle. Therefore, it can be inferred that this P_1 element may be a transitional form between *M. bidentata* and *Mi. hernsteini*.

Because the first occurrence level of transitional forms from *M. bidentata* are at the uppermost level of the Madoupo section and the lowermost portion of Potou section, it can be inferred that the layers of the Madoupo section that yielded the most conodonts (MDP7 and MDP8) are older than the sampled lower portion of the Potou section.

***Parvigondolella andrusovi* Zone** —Lower limit: FO of *P. andrusovi*. Upper limit: FO of *Mi. hernsteini* (Rigo et al., 2018) which was not found in the Potou section and the Madoupo section.

Associated taxa: *P.*? *vrielyncki* and *M. bidentata*. Below the FO of *P. andrusovi* that defines the base of this zone, a transitional form between *M. bidentata* and *P. andrusovi (*Fig. 6PP–6QQ) occurs in sample level POT11, followed by a specimen that has lost all marginal denticles (*Parvigondolella.* sp., Fig. 6RR–6SS) in sample level POT12.

In China, for a long time, *P. andrusovi* had been reported only in the Xikeng section of the Nada Hadan terrane of northeastern China (Wang et al., 1986, see Table 1). Then, Dong & Wang (2016) presented the lateral view of a broken *P. andrusovi* from the Nanshuba Formation of the Dabaozi section in Baoshan area. Zeng et al. (2021) displayed another specimen of *P. andrusovi* from the Nanshuba Formation of the Xiquelin section in the Baoshan area. The Poutou section is the third section in the Baoshan area that yields *P. andrusovi*, thereby indicating a wide distribution of this species in the Sevatian of the Baoshan area.

Systematic paleontology

Class Conodonta Pander, 1856

Order Ozarkodinida Dzik, 1976

Superfamily Gondolelloidea Lindström, 1970

Family Gondolellidae Lindström, 1970

Genus *Epigondolella* Mosher, 1968

Type species —*Polygnathus abneptis* Huckriede, 1958 from the Alaunian (*Cyrtopleurites bicrenatus* Zone) of Sommeraukogel, Austria.

Remarks —Genus *Epigondolella* is characterized by strongly denticulate anterior and posterior lateral platform margins, by a high blade with most part or even the whole free from the platform, by anteriorly located or rarely sub-centrally positioned cusp and pit, and by a single keel with either a pointed, rounded, blunt, obliquely truncated, or squared or sinuous keel end which may bear a vestige of the secondary keel on one side.

The characteristics of the base of Norian conodonts are considered to be very important in the taxonomy of the genus (Ishida and Hirsch, 2001; Orchard., 2018) because changes in the bases reflect the evolution of Late Triassic conodonts (Kozur, 1990; Giordano et al., 2010; Bertinelli et al., 2016; Karádi et al., 2020). Orchard (2018) classified lower Norian ornate P_1 elements with a bifid keel into *Ancyrogondolella*, and mid-Norian ornate and asymmetric or less commonly symmetric P_1 elements with a single keel (pointed, or squared-off, or obliquely truncated or sinuous) into *Epigondolella*, which reconstructs the phylogeny between genera *Ancyrogondolella* and *Epigondolella*. In the light of the fact that bifid-keeled ornate P_1 elements were mostly substituted by single-keeled ornate P_1 elements from the early Norian to the late Norian and by the abundant single-keeled ornate P_1 elements from the upper Norian of Baoshan area (Potou, Madoupo and the Xiquelin sections in Zeng et al., 2021), we follow the definition of *Epigondolella* as revised by Orchard (2018). But the symmetry of the posterior platform was not differentiated in genus *Epigondolella* and there might be intraspecific differences.

Epigondolella carinata Orchard, 1991b

Figures 3A–3T

1983 *Epigondolella postera* (Kozur and Mostler) population; Orchard, p. 186–188, figs. 11A, C.
1991b *Epigondolella carinata* n. sp.; Orchard, p. 308, pl. 5, fig. 4, 5, 10.
2007 *Epigondolella carinata* Orchard; Carter & Orchard, pl. 2, figs. 15, 21.
?2007b *Epigondolella carinata*; Orchard et al., fig. 8.14–8.15.
2020 *Mockina carinata*; Du et al., figs. 3.1–3.2, 3.5.
2020 *Mockina* sp.; Du et al., figs. 3.10–3.11.

Materials —Five P_1 elements from MDP7, two P_1 elements from MDP8, two P_1 elements from MDP10, two P_1 elements from POT1.

Description —The P_1 elements have an ovoid platform bearing two and one high denticles respectively on each anterior lateral margin. The posterior marginal denticles increase in number as the element posteriorly grows longer. The length ratio of the platform-to-element is about four sevenths. The blade is as long as half of the element and most of it is free from the platform. The posterior-most and anterior-most denticles of the blade are commonly smaller and lower than other denticles, which are of similar height; therefore the blade gradually transitions to the low carina, which consists of three to four discrete nodes. There are two to three carinal nodes behind the anteriorly located cusp. The posterior carinal nodes may extend beyond or near the pointed platform end, and increase in height and inclination after the cusp. The pit is anteriorly migrated and is located on a medium wide keel, which is posteriorly prolonged. The keel end is pointed to narrowly rounded.

Comparison —*Epigondolella passerii* has a platform constriction. *E. englandi* and *E.* aff. *englandi* have only one high marginal denticle on each platform side. *M. postera* has an asymmetrical posterior platform and a posterior carina that never reaches to the platform end. *M. medionorica* has smooth posterior platform margins and a short posterior carina that always stops before the platform end.

Remarks —The P_1 elements resemble *E. carinata* in the marginal denticulation and platform shape, and only differs in having a larger size and longer blade and free blade. The longer blade and free blade may be intraspecific difference. This species, for a long time, was only reported in North America. The occurrence of this species in the Hongyan (Du et al., 2020), Potou and Madoupo sections on the Baoshan Block indicates that it is also present in Sevatian strata of eastern Tethys and hence is probably a global species.

Occurrence —Sevatian (*M. bidentata* Zone) in the Nanshuba Formation of the Madoupo section and in the Dashuitang Formation of the Potou section, China (this study). Sevatian in the Nanshuba Formation of the Hongyan section (Du et al., 2020). Sevatian to early Rhaetian? at Kennecott Point on Queen Charlotte Islands, Canada (Carter & Orchard, 2007). Middle Alaunian in the Pardonet Formation of Pardonet Hill, British Columbia, Canada (Orchard, 1991b).

Stratigraphic range —Middle Alaunian to Sevatian.

Epigondolella aff. *englandi* Orchard, 1991b

Figures 4X–4LL, 5CC–5EE

2019 *Mockina englandi* (Orchard, 1991); Wang et al., p. 87, figs. 6.2–6.3.

Materials —Five specimens form POT1, one specimen from POT8, two specimens from MDP7, one specimen from MDP10.

Description —The P_1 elements are characterized by a long free blade and a relatively short platform, as well as the symmetrically arranged marginal denticles. The platform is commonly ovoid and sub-symmetrical. The posterior platform is pointed. The anterior-most pair of marginal denticles are the highest, and the following pairs of marginal denticles decrease in height and are more posteriorly inclined and outwardly projected. The blade is very high and comprised of six to seven highly fused denticles which are low at both ends and hence gradually transition to the low carina on the platform. The free blade is nearly as long as half of the element. The carinal nodes are discrete and extend to or within the posterior platform edge. There are two to three carinal nodes behind the anteriorly located cusp. The anterior groove beneath the blade is widely opened. The pit is strongly anteriorly shifted. The keel end is commonly pointed and posteriorly prolonged, and rarely keeps remnant secondary keels which are weakly and asymmetrically bifurcated. The form with a weakly bifid keel end bears three pair of marginal denticles, which may represent an intermediate form between an ancestor and the *E.* aff. *englandi*.

Comparison —*Epigondolella carinata* bears two and one anterior marginal denticles respectively on the outer platform and the inner platform. *Ancyrogondolella equalis* has a bifurcated keel end and a rectangular platform, and its marginal denticles are not asymmetrically arranged.

Remarks —The P_1 elements resemble *E. englandi*, but are distinguished from the latter by the development of a longer blade and free blade, and by having more numerous posterior marginal denticles or a weakly bifurcated keel end; however, these probably have an affinity to those of *E. englandi*. Wang et al. (2019) presented two specimens of *E. englandi* which are also from Baoshan block that have longer blade and free blade than the holotype of *E. englandi*,. Therefore, this form of P_1 elements is widely distributed in the Sevatian of the Baoshan block; indicating the occurrence may be geographically limited and hence this type of conodont might be a subspecies of *E. englandi*.

Occurrence —Sevatian (*M. bidentata* Zone) of the Dashuitang Formation and the Nanshuba Formation, China (in this study). Sevatian of the Dashuitang Formation in the Hongyan Section, Baoshan city, China (Wang et al., 2019).

Stratigraphic range —Sevatian.

Epigondolella passerii (Rigo and Du, 2022)

Figures 4A–4S

1980 *Epigondolella postera* Kozur and Mostler; Krystyn, pl. 13, fig. 17–18.

?1990 *Epigondolella postera*; Wang and Wang, pl. 1, fig. 10.

2003 *Mockina* cf. *carinata* (Orchard); Channell et al., fig. 3A/12.

2022 *Mockina passerii* n. sp. Rigo and Du; Jin et al., figs. 4.10–4.12.

Materials —Ten P_1 elements.

Description —The slender P_1 elements have a thin and biconvex platform with a pronounced constriction after a pair of highest anterior marginal denticles. The platform end is pointed. The anterior platform possesses two to three denticles on the outer margin and one to two denticles on the inner margin. The posterior platform is narrower than the anterior platform and bears a pair of unevenly developed and outwardly projected denticles on each margin. The blade is high and longer than half of the element, consisting of seven to eight highly fused denticles and hence forming a crest shape and gradually transitioning to the cusp. The cusp is located on the anterior platform and is generally followed by two to three posteriorly inclined carinal nodes. The posterior carina extends to, beyond or within the platform end. The pit is situated under the anterior platform in a narrow keel. The keel end is posteriorly prolonged and pointed.

Comparison —*Epigondolella serrulata* possesses more marginal denticles on the platform and a weaker constriction after a pair of highest anterior marginal denticles. The anterior platform of *E. englandi* possesses only one pair of unevenly developed marginal denticles on each side. *E*. aff. *englandi* has sub-symmetrically arranged marginal denticles and an oval platform with no constriction. *E. carinata* has no or very weaker constriction on the middle part of the platform.

Occurrence —Lower Sevatian (*M. bidentata* Zone, this study) in the Dashuitang Formation and the Nanshuba Formation of Potou section, Baoshan city, China. Sevatian at Sommeraukogel of Austria (Krystyn, 1980). Sevatian in the Dashuitang Formation of Hongyan-B section, Baoshan city, SW China (Jin et al., 2022).

Stratigraphic range —Sevatian.

Genus *Mockina* Kozur, 1990

Type species —*Tardogondolella abneptis postera* Kozur and Mostler, 1971 from the middle Norian of Sommeraukogel, Austria.

Remarks —Compared with *Epigondolella*, *Mockina* is characterized by nearly smooth lateral posterior platform margins which may sparsely develop small nodes.

Mockina bidentata (Mosher, 1968)

Figures 5FF–5II, 6A–6JJ, 6DDD, 7U–7CC

1958 *Polygnathus abneptis* n sp.; Huckriede, p. 156, pl. 14, figs. 32, 58.
1968a *Epigondolella bidentata* n. sp.; Mosher, p. 936, pl. 118, figs. 31-35.
1972 *Metapolygnathus bidentatus* (Mosher); Kozur, pl. 7, figs. 3–9.
1972 *Epigondolella bidentata* (Mosher); Kozur & Mostler, pl. 4, figs. 3-5.
1980 *Metapolygnathus bidentatus*, Kovács & Kozur, pl. 15, fig. 1.
1980 *Epigondolella bidentata* Mosher, Krystyn, pl. 14, figs 1-3.
1983 *Epigondolella bidentata* population, Orchard, fig. 14 O-Q, S, W, X, fig. 15W, X.

1985 *Epigondolella bidentata*; Wang and Dong, p. 127–128, pl. 1, figs. 1–3, 26.
1991b *Epigondolella bidentata*; Orchard, p. 307-308, pl. 4, fig. 12.
2003 *Mockina bidentata* (Mosher); Channell et al., pl. A2, figs 44, 46-48, 51, 54; pl. A3, figs 3, 4, 6, 7, 9, 25, 27, 28, 37, 39, 41, 42, 47, 48, 50, 54, 56, 71, 72, 74-79.
2005 *Epigondolella bidentata*; Bertinelli et al., fig. 4/5.
2005 *Epigondolella bidentata*; Rigo et al., fig. 4/6.
2005 *Epigondolella* ex gr. *bidentata* Orchard; Hornung, p. 111, pl. 1, fig. e.
2007 *Mockina bidentata*; Moix et al., p. 294, pl. 2, figs. 2, 3.
2007 *Epigondolella bidentata*; Carter and Orchard, pl. 2, figs. 14, 22–25.
2007a *Epigondolella bidentata*; Orchard et al., figs. 8.10, 8.11, 8.13, 8.17–8.20.
2007b *Epigondolella bidentata*; Orchard et al., pl. 1, fig. 22.
2007 *Epigondolella bidentata*; Krystyn et al., pl. 1, figs 5, 6; non pl. 1, figs 7-14.
2009 *Epigondolella bidentata*; Rožič et al., fig. 9 e.
2010 *Mockina bidentata*; Giordano et al., fig. 3/1, 3/2.
2012 *Mockina bidentata*; Mazza et al., p. 120, pl. 7, fig. 7.
2012 *Epigondolella bidentata*; Gallet et al., fig. 3.1.
2016 *Mockina bidentata*; Rigo et al., fig. 3/3.
2016 *Mockina bidentata*; Karádi et al., pl. 1, fig. 8; pl. 4, fig. 4.
2018 *Mockina bidentata*; Yamashita et al., p. 183, figs. 8.4–8.5
2020 *Mockina bidentata;* Karádi et al., fig. 5 S.
2020 *Mockina bidentata*; Du et al., figs. 3.6, 3.15.
2021 *Mockina bidentata*; Du et al., figs. 3.1, 3.2.
2021 *Mockina bidentata;* Zeng et al., figs. 1/b, 2/2b, 3/1n–1o, 4/3d
2022 *Mockina bidentata*; Jin et al., figs. 4.13–4.15.

Materials —31 P_1 elements.

Description —Platform is short and reduced and varies in width. One pair of denticles are located on the anterior platform margins, after which the platform changes from extremely reduced to moderately reduced. The pair of marginal denticles are either both developed on two sides of the unit or are both absent in the early juvenile element. The blade varies in length and consists of four to nine denticles, which are fused to different degrees. The denticles of the blade may be high in the middle and lower on both ends or high on the anterior and gradually descending posteriorly. The cusp is located in a position parallel with the line of marginal denticles and is followed by one to three additional carinal nodes. The pit is situated beneath the cusp. The keel end is prolonged relative to the pit and pointed. In lateral view, the basal edge is sub-straight or is slightly concave beneath the transition between the blade and the platform. Two specimens from Madoupo section (Figs. 5FF–5II) have a convex basal edge in lateral view and a broad platform.

Remarks —Specimens of various *M. bidentata* present a possible evolutionary trend for this species from the early or middle Sevatian to the late Sevatian. On the basis of different features of the carina in *M. bidentata*, Moix et al. (2007) discerned two morphotypes of *M. bidentata*, and these are also present in *M. bidentata* fauna from the Potou section. One morphotype (Figs. 6W–6EE) resembles the holotype with a long anterior blade consisting of many highly fused denticles

and a long posterior carina of three nodes. The highest occurrence of this morphotype (POT8) in the Potou section is below the FO of *P. andrusovi*, which contrasts with its re-appearance within *Mi. hernsteini-P. andrusovi* Zone observed by Moix et al. (2007). The second, somewhat smaller, morphotype with a shorter blade consisting of less fused and few relatively big and wide denticles is below both the occurrences of the other morphotype of *M. bidentata* and of the *M. bidentata*/*P. andrusovi* transitional form and *P. andrusovi* in several Tethyan sections and on the Tavusçayırı Block (Moix et al., 2007). The occurrence level of this second morphotype of *M. bidentata* in the Potou section (Figs. 6A–6H, 6L–6V) is similar to the inferred level below the *Mi. hernsteini-P. andrusovi* Zone. *M. bidentata* increases in size from the sample layer 1 (POT1) to sample layer 8 (POT8), then reduces its size just below the occurrence of *M. bidentata*/*P. andrusovi* transitional forms (from sampling layer POT11 to POT13).

At present, *M. bidentata* has been widely reported in the Tethys (Channell et al., 2003; Krystyn et al., 2007; Moix et al., 2007; Giordano et al., 2010; Mazza et al., 2012; Karádi et al., 2020; Du et al., 2020, 2021; Zeng et al., 2021; Jin et al., 2022), in North America (Mosher, 1968; Orchard, 1983, 1991b; Orchard et al., 2007a, b; Carter and Orchard, 2007) and in Japan (Yamashita et al., 2018). All the illustrated specimens from these publications display a narrow platform and straight or slightly concave basal edges in lateral view, which conform to the holotype. It is noteworthy that three bidentate specimens from the Madoupo section differ from the bidentate P_1 elements from the Potou section and from other *M. bidentata* in the Madoupo section by having distinct convex rather than sub-straight basal edges in lateral view and possessing broader platforms (Figs. 5FF–5II); but more data are needed to confirm whether the different morphologies are intraspecific.

Stratigraphic range —from lowermost Sevatian to (middle?) Rhaetian.

Mockina elongata (Orchard, 1991b)

Figures 5A-5X

1991b *Epigondolella elongata* n. sp.; Orchard, p. 308, pl. 4, figs. 4–6, 15, 20, 21.

2005 *Epigondolella elongata* Orchard, 1991; Rigo et al., fig. 4.4.

2018 *Mockina elongata* (Orchard, 1991b); Yamashita et al., p. 183, figs. 8.6, 8.7.

2022 *Mockina mosheri* morphotype B; Jin et al., fig. 4.8.

Materials —28 P_1 elements from MDP8.

Description —The platform after the anterior marginal denticles gradually tapers to the pointed platform end, to form a long elliptical outline. The smooth posterior platform is relatively wider on the inner sider than the outer side, but both margins are convex in outline. The length ratio of the platform to the element is about three fifths. The anterior platform bears two or three high denticles on one margin and one higher denticle on the other. The blade consists of six to seven high denticles with the basal part fused and the upper part discrete. The anterior-most or posterior-most denticle of the blade may be relatively smaller or lower, and thus the blade moderately or abruptly decreases to the low carinal nodes on the platform. The low carina consists of four to five discrete posteriorly inclined nodes, commonly extends beyond the platform end or aligns with the terminal marginal denticle, and rarely has the posterior two carinal nodes fused with the terminal marginal denticle. The cusp is usually higher than the adjacent carinal nodes and is followed by three to four carinal nodes with the last one being the

largest. The cusp located on the anterior platform is approximately aligned with the middle position of the two to three marginal denticles. The keel extends along the platform and terminates at three fifths along the posterior platform. The keel after the pit is straight to slightly curved. The keel end is pointed or lanceolate and prolonged far from the pit. The pit is located below the cusp at about the anterior third of the platform.

The juvenile forms are much smaller in size and have the same ratio of platform length to the unit length. The carina of juvenile specimens consists of four high denticles (blade) and four lower carinal nodes. The keel grows along the platform, and both have pointed ends. The pit in the juvenile form is located beneath the anterior platform and surrounded by a bulged loop.

Comparison —*Mockina postera* has a shorter platform, an apparent asymmetrical posterior platform and a shorter posterior carina that never reaches the platform end. *M. matthewi* has at least two anterior platform marginal denticles and a broader platform. *M. medionorica* has a smooth platform end and a shorter posterior carina that also never reaches the platform end. *Orchardella*? *multidentata* has more anterior marginal denticles and a stronger posterior carina.

Remarks —All P_1 elements have an elongate ellipsoid platform with two to three denticles on one anterior platform margin, with one denticle on the other margin and with an inornate posterior platform. The pit is anteriorly shifted, and prominent carinal nodes usually extend to the posterior platform end or occasionally not. Although the holotype of "*Epigondolella*" (= *Mockina*) *elongata* (Orchard, 1991b, pl. 4, fig. 15, 20, 21) has a slenderer, longer platform and more posteriorly elevated carinal nodes than these P_1 elements, the morphological features of the P_1 elements match well with the description in the "Diagnosis" of *M. elongata* and resemble the paratype (Orchard, 1991b, pl. 4, fig. 4–6).

The occurrence of *M. elongata* is global, as indicated by the occurrence of this species in western Tethys (Rigo et al., 2005), in eastern Tethys (Jin et al., 2022; and this study), in the Panthalassa (Yamashita et al., 2018) and in North America (Orchard, 1991b).

Occurrence —Lower Sevatian in the Madoupo section. Middle Alaunian in the British Columbia, North America (Orchard, 1991b). Upper Alaunian in the Sasso di Castalda section of southern Italy (Rigo et al., 2005). Lower Sevatian (*M. bidentata* Zone and occurrence within radiolarians zone TR6B (*Tnalatus robustus-Lysemelas olbia*) through TR7 (*Lysemelas olbia*) and disappearance in lower TR8A (*Praemesosaturnalis multidentatus*) in the section Q of Japan (Yamashita et al., 2018). Sevatian in the Dashuitang Formation of the Honyan-B section, Baoshan area, western Yunnan, China (Jin et al., 2022).

Stratigraphic range —from middle Alaunian to lower Sevatian.

Mockina medionorica Kozur, 2003

Figures 5Y–5BB

1980 *Metapolygnathus multidentatus* (Mosher); Kovács & Kozur, pl. 14, fig. 5.

1987 *Metapolygnathus posterus* (Kozur and Mostler); Vrielynck, p. 157–159, pl. 7, Figs. 10–15.

2001 *Mockina postera* (Kozur & Mostler); Ishida & Hirsch, p. 238, pl. 4, figs. 4, 6.

2002 *Mockina postera*; Hirsch & Ishida, pl. 1, fig. 3.

2003 *Mockina medionorica* n. sp.; Kozur, p. 70, pl. 1, figs. 5, 6.

2003 *Mockina medionorica* Kozur; Channell et al., pl. A3/14–15.
2021 *Mockina medionorica*; Karádi et al., p.16, fig. 7.13.

Materials —Two P_1 elements.

Description —The P_1 elements have an oval platform that possesses two and one marginal denticles on each anterior platform side. The platform margins after the anterior marginal denticles are smooth. The blade consists of seven half-fused denticles. Most of the blade is free from the platform. The posterior two denticles of the blade decrease in height toward the posterior and hence gradually descend to the low carina. The low carina consists of 4 isolated nodes, with the last carinal node being largest and stopping before the smooth platform end. The pit located under the anterior platform. The keel is pronged after the pit. The keel end is pointed. In lateral view, the base is stepped upwards at the transition between the blade and the platform and become sub-straight after the cusp.

Comparison —*Mockina postera* has an asymmetrical posterior platform and a pointed platform end. *M. elongata* has a pointed platform end and longer carina after the cusp. *M. slovakensis* differs from it by the blade abruptly descends to the low carina on the platform. *M. matthewi* has 2 or more anterior marginal denticles on each platform side.

Remarks —Kovács & Kozur (1980, pl. 14, fig. 5) presented a specimen of *Metapolygnathus* (*Me.*) *multidentatus*. However, the displayed specimen differs from *Me*. *multidentatus* by the broader posterior platform, smooth platform end and a shorter posterior carina that never extends to the platform end. It resembles *M*. *matthewi* by the two pairs of anterior marginal denticles, broad platform, smooth posterior platform margins and the carina, but differs from the latter by the keel end that is narrowly blunt with slight central incision. This kind of keel end was described in the diagnosis of *M*. *medionorica.* Karádi et al. (2021, p. 16) assigned this specimen to *M*. *medionorica* and proposed that *M*. *matthewi* has a broadest platform in the middle. Taking the broadest anterior platform and the centrally incised keel end into consideration, the specimen of *Me*. *multidentatus* in Kovács & Kozur (1980) conforms more to *M. medionorica*.

Occurrence — Lower Sevatian in the Madoupo section. Alaunian in the Rudabánya hills, Hungary (Kovács & Kozur, 1980). Upper Alaunian in Cammarata of Sicily, Italy (Vrielynck, 1987). Alaunian in the section of Hisaidani, southwestern Japan (Ishida & Hirsch, 2001; Hirsch & Ishida, 2002). Alaunian of Silická Brezová, Slovakia (Kozur, 2003; Channell et al., 2003). Lower Alaunian in the Dovško section of Slovenia (Karádi et al., 2021).

Stratigraphic range —from lower Alaunian to Sevatian.

Mockina zapfei (Kozur, 1973)
Figures 3RR–3SS, 7A–7O, 7DD, 8A–8EE, 9A–9BB

1972 *Metapolygnathus* n. sp.; Kozur, pl.7, fig.1.
1972 *Metapolygnathus* aff. *posterus* (Kozur & Mostler); Kozur, pl. 7, fig. 2.
1973 *Metapolygnathus zapfei* Kozur & Mostler; Kozur, p. 18-20.
1979 *Metapolygnathus zapfei* Kozur; Gaździcki et al., pl. 5, fig. 15.
1983 *Epigondolella postera* population (Kozur and Mostler); Orchard, p. 186, figs. 15 P–R.
1985 *Epigondolella multidentata* Mosher; Wang and Dong, p. 128, pl. 1, figs. 9, 16.
1990 *Epigondolella postera*; Buduro & Sudar, pl. 5, fig. 6-8.
?1991a *Epigondolella postera*; Orchard; pl. 4, figs. 17, 18.
2000 *Epigondolella slovakensis* Kozur and Mock; Martini et al., pl. V, fig. 13-14.
2003 *Mockina zapfei;* Channell et al., pl. A2, figs. 43, 45, 53, 55; pl. A3, figs. 5, 24, 32, 33, 34, 36, 43, 51, 52, 53.
2005 *Epigondolella* ex gr. *bidentata* Orchard; Hornung, p. 111, pl. 1, fig. B (only).
?2005 *Epigondolella serrulata* Orchard, 1991; Rigo et al., fig. 4.3.
2021 *Mockina zapfei*; Du et al., fig. 3.12.
2022 *Mockina zapfei*; Jin et al., fig. 4.6.

Materials —60 P_1 elements from MDP8, one P_1 element from MDP10.

Description —The P_1 elements have a long platform which spans more than half of the entire element, and is always with one side of the posterior platform margin deflecting toward the other side near the platform end. The platform width is from slender to broad, posteriorly elongating during the growth and thus developing a longer posterior platform in adult forms or late forms. The anterior platform bears one to three high denticles on one lateral margin and always one strong and highest denticle on the other. The posterior platform margin is commonly smooth and asymmetric, with the deflected side of the platform wider than the other side. The blade spans nearly half of the element and commonly consists of five to eight highly fused denticles in adult elements, but with most denticles free from the platform. The denticles of the blade are commonly similar in height except the anterior-most one or two denticles which are smaller or lower. The posterior one to two denticles of the blade may decrease in height or size, or commonly in adult or late adult specimens the posterior-most denticle may be abrupt. The cusp is located on the anterior platform and is commonly followed by two or more carinal nodes which increase in height toward the posterior and extend to or within the posterior platform end. The keel is wide around the pit and tapers posteriorly. The keel end is commonly lanceolate in shape and posteriorly prolonged; it deflects toward one side, and terminates at the posterior fourth of the platform. Besides these common morphological features, the abundant population of this taxa collected from MDP8 also allows us to reconstruct the ontogenetic series and to study intraspecific variations, which are presented mainly in Figures 7–9.

The most common form (Figs. 3RR–3SS, 7A–7C, 8A–8T) resembles the holotype in having a wide platform with one posterior margin deflecting toward the other side near a broadly rounded platform termination. The ontogenetic series of this form (Figs. 8A–8T) reveals that the platform simultaneously posteriorly elongates and laterally expands during the growth. The posterior platform is narrower than the anterior platform during the early growth stage (=in juvenile specimens) and gradually laterally expands until the width of posterior platform is similar to or slightly wider than the anterior platform as the element grows. An apparent

identification feature of this form through all the growth stages is that a sudden deflection from the sub-straight platform margin to the pointed platform end occurs near the platform termination, which becomes more distinct as the element grows larger.

The other common form (Figs. 9A–9Y) is characterized by a smooth, rather than sudden, deflection of one platform margin from the anterior to the posterior. Commonly, the platform after the anterior marginal denticles forms a concave outer margin and a convex inner margin which may culminate in a sub-straight edge as the element laterally expands during the late growth stage. The ontogenetic series (Figs. 9A–9L, 9R–9Y) all show a gradual bending of the lateral platform margins after the anterior marginal denticles and the curvature of the carina after the cusp. The outer anterior margin of this form may bear one to three denticles, which increase in height toward the posterior.

Variations observed in rare morphotypes include: (1) a narrow-rounded platform end rather than typical pointed platform end and relatively sub-straight posterior carina and keel (Figs. 8U–8Y); (2) development of small nodes on the deflected posterior margin and platform end to form a denticulated platform termination (Figs. 8Z–8EE); (3) anteriorly increased marginal denticles with one lateral margin bearing four high denticles and the other margin having two denticles (Fig. 9Z–9BB); (4) retention of a weakly asymmetrically bifurcated keel and many fused and continuously aligned lower carinal nodes that extend to the sub-middle platform end (Fig. 7D–7F); and (5) possession of two denticles on each anterior platform margin (Figs. 7G–7O, 7DD).

Comparison —Adult *M. zapfei* is easy to differentiate from *M. postera* (Kozur and Mostler, 1971) by its larger size, longer platform, and distinct curved carina that extends to or is aligned with the pointed platform end. *M. zapfei* in its early growth stage is very similar to *M. postera* in that the curvature of the carina and the deflected posterior platform margin is not as pronounced as those for its adult elements. However, the juvenile specimens of *M. zapfei* recovered from the Madoupo section either have a carina that extends to the platform end or have an apparently curved posterior platform and posterior carina; and these features contrast with the straight posterior carina that never reaches the posterior platform end of *M. postera*. Because the juvenile *M. zapfei* specimens are easily confused with *M. postera*, careful caution should be exercised when identifying them. The *M. zapfei* morphotype with a narrowly rounded platform end (Figs. 8U–8Y) resembles *M. slovakensis*, but is differentiated by its broad deflected posterior termination and the posterior blade which fuses with a low carinal node on the platform and hence has a moderate rather than an abrupt step down to the platform. That morphotype may be an intermediate form between *M. slovakensis* and *M. zapfei*. The variant morphotype with a bifid keel (Fig. 7D–7F) shares similar upper morphological features with the *M.* aff. *zapfei* in Yamashita et al. (2018), but the latter has a gradually declined blade and a symmetrical bifid keel which bifurcates straightly posterior to the pit; and those traits contrast with the abruptly declined posterior blade and asymmetrical bifid keel which bifurcates far from the pit in this *M. zapfei* morphotype.

Remarks — The most common form of the P_1 elements almost perfectly matches the description and holotype of *M. zapfei* presented by Kozur (1972, 1973). Other common forms and rare morphotypes also display the common characteristics as described by Kozur (1972). No additional detailed descriptions of *M. zapfei* with figures have been presented in papers since the report of the holotype (Channell et al., 2003; Rigo et al., 2016; Karádi et al., 2020; Jin et al., 2022). The only description of *M. zapfei* other than the holotype has no corresponding figures

(Mazza et al., 2012). The abundant specimens collected from level MDP8 allow us to present a detailed illustrated description as well as the field of variation for this species. Intraspecies variations are mainly in the denticulation of anterior platform margins, in the characteristics of the deflection in one posterior platform margin and the posterior carina, and in the features of posterior platform termination or end. *M. zapfei* has been discovered in North America (Orchard, 1983), in the Tethyan realm (Kozur, 1972, 1973; Wang and Dong, 1985; Channell et al., 2003; Hornung, 2005; Balini et al., 2010; Mazza et al., 2012; Du et al., 2021; Jin et al., 2022; this study), in Timor (Martini et al., 2000), and probably in Japan (Yamashita et al., 2018), thereby indicating a global distribution.

Occurrence —Sevatian in the Nanshuba Formation of the Madoupo section, Baoshan city, China. Uppermost Alaunian in the Dashuitang Formation of the Dapingdi section (Wang & Dong, 1985) and the Hongyan-B section, Baoshan city, China (Jin et al., 2022). Sevatian of the Pizzo Mondello section in Sicily, Italy (Du et al., 2021). Sevatian in the Rappoltstein section of Rappoltstein Block, southern Germany (Hornung, 2005). Sevatian in the Trench section of Silická Brezová, Slovakia (Channell et al., 2003). Middle? Alaunian in the Noe Bihati section of West Timor (Martini et al., 2000). Middle Alaunian in the Pardonet Formation of the McLay Spur section in British Columbia, Canada (Orchard, 1983). Upper Alaunian of Sommeraukogel, Austria (Kozur, 1972, 1973).

Stratigraphic range —Middle Alaunian to middle Sevatian.

Mockina sp. A

Figures 7P–7T

2005 *Epigondolella postera* (Kozur & Moster, 1971); Bazzucchi et al., fig. 11.1.

2016 *Mockina zapfei* (Kozur); Rigo et al., fig. 3.1.

Materials —Three P_1 elements from MDP8.

Description —The P_1 elements are characterized by a deflected posterior platform relative to the anterior platform, which is smooth and bears a rounded platform end. The P_1 elements are widest on the anterior platform where the marginal denticles grew. The outer platform begins to taper after two marginal denticles, while the inner platform starts to slightly and gradually expand until or near the posterior termination and then tapers to the posterior termination. The anterior platform possesses two high denticles and one highest denticle respectively on the two lateral margins. The blade generally consists of five to six half-fused denticles, with some denticles being very wide. The denticles of the blade is high in the middle and lower on both ends and hence gradually or moderately descends to the low carina toward the posterior. The low carina is commonly comprised of five nodes. The cusp located on the anterior platform is slightly anterior to the position of the posterior-most marginal denticles, and is followed by three carinal nodes. The posterior carina deflects inward and extends to or beyond the platform termination. The pit is located beneath the cusp and within a wide keel. The keel end can be slightly wavy, blunt or narrowly rounded. In lateral view, the basal edge is upwardly stepped beneath the transition between the blade and the low carina.

Comparison —Epigondolella carinata develops a terminal denticle on the platform end and lateral marginal denticles on two sides of the posterior platform. *M. elongata* has a pointed platform end and a narrower posterior platform. *M. slovakensis* has a blade that is abrupt in the posterior end and consists of highly-fused denticles. *M. medionorica* has similar rounded or narrowly rounded posterior platform end and denticulation of the anterior platform, but can be distinguished by the straight posterior carina which never reaches the posterior end as well as the sub-symmetric posterior platform. *M. postera* has a pointed platform end, an asymmetric posterior platform and a straight carina that doesn't extend to the posterior platform end.

Remarks —The P_1 elements are similar with *M. zapfei* (Figs. 8U-8Y). But the deflection pattern presented in the three specimens is different from that of *M. zapfei*. The platform margin after two anterior marginal denticles smoothly tapers to the platform end in the P_1 elements, contrasting with the corresponding sub-straight margin of *M. zapfei*. The other platform margin after one high anterior marginal denticle always presents a distinct deflection at the posterior fourth of the platform in *M. zapfei,* which is not displayed in the P_1 elements. The P_1 elements have the whole posterior platform variably deflected toward the inner side relative to the anterior platform, whereas most specimens of *M. zapfei* have only one posterior margin deflected toward the outer side near the platform end.

Occurrence —Lower Sevatian (*M. bidentata* Zone in this study) in the Nanshuba Formation of the Madoupo section, China. Sevatian 1 in the Scisti Silicei Formation of the Pignola-Abriola, Italy (Bazzucchi et al., 2005; Rigo et al., 2016).

Stratigraphic range — Sevatian.

Genus *Parvigondolella* Kozur and Mock, 1972

Type species —Parvigondolella andrusovi Kozur and Mock, 1972 from upper Sevatian of Bohúňovo, Slovakia.

Parvigondolella andrusovi Kozur and Mock, 1972

Figure 6TT–6UU

1972 *Parvigondolella andrusovi* n. gen. n. sp.; Kozur & Mock, p. 5, pl. 1, fig. 11, 12.
1974 *Parvigondolella andrusovi* Kozur & Mock, 1972; Kozur and Mock, pl. 1, figs. 11–12.
1979 *Parvigondolella andrusovi*; Gaździcki et al., pl. 5, figs 8, 9.
1980 *Parvigondolella andrusovi*; Kovács and Kozur, pl. 15, fig. 3.
1980 *Epigondolella bidentata* Mosher; Krystyn, pl. 14, fig. 5, 6.
1990 *Epigondolella bidentata* Mosher, 1968; Budurov and Sudar, pl. 5, fig. 12.
2003 *Parvigondolella andrusovi*; Channell et al., pl. A2, figs. 50, 60; pl. A3, figs. 1, 2, 73, 81–82.
2005 *Parvigondolella andrusovi*; Bertinelli et al., fig. 4/6.
2005 *Parvigondolella andrusovi*; Rigo et al., figs 5.5, 5.6.
2007 *Epigondolella* sp; Pálfy et al., fig. 6.14.
2009 *Parvigondolella andrusovi*; Rožič et al., fig. 9/g.

2010 *Parvigondolella andrusovi*; Giordano et al., fig. 3.4.
2010 *Parvigondolella andrusovi*; Balini et al., pl. 4, fig. 10.
2012 *Parvigondolella andrusovi*; Mazza et al., p. 126, pl.7, fig. 14.
2012 *Parvigondolella andrusovi*; Gale et al., fig. 4/O.
2018 *Parvigondolella andrusovi*; Yamashita et al., 2018, p. 189, fig. 10.4.
2020 *Parvigondolella andrusovi*; Karádi et al., fig. 2 D–E, fig. 5 T, U.
2021 *Parvigondolella andrusovi*; Du et al., fig. 3. 6.
2021 *Parvigondolella andrusovi*; Zeng et al., figs. 1/e, 4.3.

Material —One specimen from POT13

Description —A single blade consists of seven partially fused denticles. The most anterior denticle is small and erect; other denticles incline posteriorly and decrease in height toward the posterior end. The cusp is penultimate and wider than other denticles, and located at the posterior third of the element. The pit is located below the cusp. The groove is anteriorly shallow and narrow; while the keel end is prolonged and narrowly rounded.

Comparison —It differs from *Parvigondolella* sp. (described below) in its widest cusp. *M. bidentata* has a reduced and short platform with a pair of marginal denticles or is small in size in early juvenile elements. *P. lata* bear a terminal cusp and fewer denticles. *P. ciarapicae* has a terminal cusp which is the largest denticle of the blade.

Remarks —The P_1 element has seven denticles, a widest cusp which is situated at the posterior third of the element, and a base with distinct pit, posterior keel and shallow groove. These morphological features match well with the illustration of *P. andrusovi* by Kozur and Mock (1972, pl. 1, fig. 12).

Occurrence —Upper Sevatian of Silická Brezová, Slovakia (Kozur & Mock, 1972, 1974; Gaździcki et al., 1979; Kovács and Kozur, 1980). Sevatian of Sommeraukogel, Austria (Krystyn, 1980). Upper Sevatian of the Kavur Tepe section, Antalya, Turkey and the Scheiblkogel section in Austria (Channell et al., 2003). Sevatian of the Pizzao Mondello section in Italy (Balini et al., 2010; Mazza et al., 2012). Upper Sevatian in the Calcari con Selce Formation of the Pignola-Abriola section, Mt. S. Enoc section and Mt. Volturino section in the Lagonegro Basin, Italy (Giordano, 2010; Karádi et al., 2020). Sevatian to the Rhaetian in the Calcari con Selce Formation – transitional interval of the Sasso di Castalda section in the Lagonegro Basin, Italy (Bertinelli et al., 2005; Rigo et al., 2005; Giordano, 2010). Upper Sevatian to the Rhaetian of the Mt. Kobla section in the Slovenican Basin (Rožič et al., 2009; Gale et al., 2012). Upper Sevatian of Inuyama area, Japan (Yamashita et al., 2018). Sevatian in the Nanshuba Formation of the Xiquelin section in Baoshan, China (Zeng et al., 2021).

Stratigraphic range —Upper Sevatian to Rhaetian.

Parvigondolella? *vrielyncki* Kozur and Mock, 1991
Figures 6KK–6NN

1980 *Epigondolella bidentata* Mosher; Krystyn, pl. 14, fig. 4.
1991 *Parvigondolella*? *vrielyncki* sp. nov. Kozur and Mock, p. 276–277.
?2003 *Parvigondolella vrielyncki*; Channell et al., pl. A2, fig. 49.
?2003 *Parvigondolella andrusovi* Kozur and Mock; Channell et al., pl. A2, fig. 59, pl. A3, figs. 72, 73, 80.
?2007a *Parvigondolella* sp. B; Orchard et al., p. 363, fig. 7.17.
?2007b *Parvigondolella* sp. C; Orchard et al., pl. 1, fig. 14–15.
?2018 *Parvigondolella* aff *vrielyncki*; Yamashita et al., p. 189, fig. 10.5.

Materials —One P_1 element from POT1 and one P_1 element from POT13.

Description —The P_1 elements have a single long blade composed of 10 denticles. The anterior-most one denticle is small and erect, the others slightly inclined and the inclination gets bigger posteriorly. The anterior blade is large and high and decreases in height toward the posterior end. The cusp is the antepenultimate denticle, which is slightly wider than other denticles and situated at the posterior third of the unit. The height of the cusp is lower than its anterior denticles and higher than the posterior two closely positioned denticles. The basal furrow is narrow and shallowly excavated, extends to both ends of the unit, and expands laterally near the position beneath the cusp. In lateral view, the anterior basal edge is straight, while the posterior basal edge slightly bends downward, thereby forming a weakly arched shape.

Remarks —The groove in the P_1 elements opens and widens along the entire unit to form a narrow and shallow furrow. However, the bases in *M. bidentata,* transitional form between *M. bidentata* and *P. andrusovi* (Figs. 6PP–6QQ, 6VV–6AAA), and *P. andrusovi* are not apparently opened, widened and excavated; thereby enabling the keel, the pit (or basal cavity) and the narrow groove to be still clearly discerned. Kozur and Mock (1972) did not illustrate lower view of the holotype of *P. andrusovi* nor did they provide a clear description or diagnosis of that portion. Because most later conodont workers regarded the basal cavity of *P. andrusovi* as not indistinct, we also adopted this feature of identification. Alternatively, it is possible the two specimens are a morphotype of *P. andrusovi*. This difficulty in comparing to other taxa indicates the necessity to emphasize the development of the lower side of conodonts in that this view reveals the evolutionary process and thus plays a decisive role in separating the species and genera for Late Triassic conodont elements. Because species of genus *Parvigondolella* have a similar basal field as *M. bidentata*, which contrasts with the wholly covered basal furrow in these two specimens, then it is interpreted that the two specimens do not belong to genus *Parvigondolella*.

On the other hand, even though Krystyn (1980) only presented a lateral view for what became the holotype of *P.? vrielyncki* by Kozur and Mock (1991), the diagnosis mentioned a narrow basal furrow and an indistinct basal cavity and Kozur and Mock (1991) were also uncertain on its assignment to a genus. The basal features of these P_1 elements conform to the description of the holotype of *P.*? *vrielyncki*. Moreover, the straight edge on the anterior and slightly downwardly bending posterior edge in lateral view of the P_1 elements conform to the holotype of *P.*? *vrielyncki* (Krystyn, 1980, pl. 14, fig. 4). Therefore, on the basis of the basal furrow, lateral profile of basal edge and 10 denticles, the two P_1 elements are interpreted to be *P.*? *vrielyncki.* Four specimens presented by Channell et al. (2003, fig. A2, 59; figs. A3, 72, 73, 80) and two specimens displayed by Orchard et al. (2007a, pl. 1, figs. 14–15; 2007b, fig. 7.17) have very

similar blades and lateral views as the two P_1 elements, and all bear an antepenultimate cusp. However, those authors did not illustrate the basal cavities of those specimens, therefore a full comparison is not possible. Another *P.* aff. *vrielyncki* identified in Yamashita et al. (2018) has a crest-shaped blade and arched lateral view; but again, no lower view was presented, therefore it is not certain whether their *P.* aff. *vrielyncki* is identical with these two P_1 elements.

Occurrence —Sevatian of the Potou section in Baoshan city, China. Alaunian 2/IV (= upper *Halorites macer* Zone, which had been regarded as lower Sevatian by Kozur and Mock, 1991) of western Timor, Indonesia (Krystyn, 1980, pl. 14, fig. 4).

Stratigraphic range —Upper Alaunian to Sevatian.

Discussion

Conodont fauna in the *Mockina bidentata* Zone of the Sevatian are probably very diverse. There are at least 19 different forms of P_1 elements (see Fig. 2, Table 2), which belong to 6 different form genera within the *M. bidentata* Zone of the Potou section and the Madoupo section. This reveals a high taxonomic diversity and an apparent peak in diversification of conodonts during the early Sevatian. In the first part of this paper, the review of Sevatian conodont biostratigraphy gives a detailed account of the range of reported conodont species within the *M. bidentata* Zone. Our current compilation, which is only preliminary, of the reported conodont form species within the *M. bidentata* Zone (Table 3) suggests that there may be more than 30 different forms of P_1 elements occurring in the *M. bidentata* Zone. Many known species that occurred during middle Norian actually range upward into the Sevatian, such as *E. spiculata, M. elongata*, *M. medionorica*, *M. postera* and *E. abneptis* with no-bifid keel end. It can be inferred that other middle Norian conodonts may have survived into the Sevatian. The occurrence of ornated P_1 elements (*E. abneptis*, *E. triangularis*?, *E. uniformis*? and *M*. aff. *tozeri*) in the *M. bidentata* Zone also implies a more diverse conodont fauna was present in the Sevatian world than previously thought. More new species or new forms of P_1 elements have been discovered in the *M. bidentata* Zone in recent years, which indicates that the peak of diversification that Plasencia et al. (2013) assigned as end-Norian actually occurred during the *M. bidentata* Zone of the early Sevatian.

However, this peak in diversification during the *M. bidentata Zone* was followed by a biotic crisis during the middle of the Sevatian. The termination of conodont species ranges within the Potou section imply an apparent rapid decline in conodont diversity above sample layer POT9, and most of the higher horizons yielded only single species. This implies that there was a conodont crisis (=major decline in diversity) in the uppermost *M. bidentata* Zone or near the boundary between *M. bidentata* Zone and *P. andrusovi* Zone. The zonal boundary interval is characterized by transitional forms between *M. bidentata* and *P. andrusovi*, by the disappearance of most segminiplanate gondolellid conodonts, and by the appearance of species of *Parvigondolella (Parvigondolella* sp.*)*.

Indeed, also within the western Tethys regions, only very few conodont species occur within the *P. andrusovi* Zone. The associated assemblages are commonly *P. lata-N. steinbergensis* (Gaździcki et al., 1979), single *M. bidentata* (Rigo et al., 2005), *M. slovakensis-M. bidentata-N. steinbergensis* in the Pignola-Abriola section and *P. lata-M. bidentata-P. vrielyncki* in Mt. S. Enoc and Mt. Volturino sections (Giordano et al., 2010), *M. slovakensis-M. zapfei* (Channell et

al., 2003) with *M. bidentata-N. steinbergensis* (Balini et al., 2010; Mazza et al., 2012), and *M. bidentata-M.* ex gr. *postera-N. steinbergensis* (Rožič et al., 2009; Gale et al., 2012). These global records suggest that only four segminiplanate conodont species of *M. slovakensis*, *M. bidentata*, *M. zapfei* (with the exception of the unclear *M.* ex gr. *postera*) and *N. steinbergensis* survived from the *M. bidentata* Zone into the *P. andrusovi* Zone and that segminate conodonts (*P. lata, P. ciarapicae* etc.) commenced their radiation in the *P. andrusovi* Zone (Karádi et al., 2020). This is in contrast with the diverse conodont species discovered in the *M. bidentata* Zone of the Baoshan area (Wang et al., 2019; Du et al., 2020; Zeng et al., 2021; Jin et al., 2022) and of other early Sevatian strata around the world (Table 3). Therefore, it is obvious that conodonts suffered a significant crisis in the middle of the Sevatian.

Rigo et al. (2018) interpreted that an important bioevent corresponding to the presence of conodont genus *Parvigondolella* occurred during a warm phase (W3) of late Norian (Trotter et al., 2015). The progression of transitional form between *M. bidentata* and *P. andrusovi* (Figs. 6PP–6QQ, 6VV–6AAA) and *Parvigondolella* sp. recovered from the Potou section below the first occurrence of *P. andrusovi* allows a refined conodont biostratigraphy with an interval of transitional forms between the *M. bidentata* Zone and the *P. andrusovi* Zone that corresponds to this bioevent.

It is recommended that future studies should focus on this transitional interval spanning the uppermost *M. bidentata* Zone to onset of the *P. andrusovi* Zone to understand the underlying causes of this first crisis that heralded the end-Triassic conodont extinction interval and the relationships of conodont evolution to environment changes.

Conclusions

Conodont faunas were recovered from upper Norian (Upper Triassic) strata of the Dashuitang and Nanshuba formations in two sections near Baoshan City in western Yunnan Province. These assemblages provide important insights on the biostratigraphy and diversity history of Norian conodonts in China as well as throughout the Tethyan realm. Conodont *Mockina* (*M.*) *bidentata* Zone and *Parvigondolella* (*P.*) *andrusovi* Zone are identified in this area, thereby greatly improving the resolution of the Sevatian biochronostratigraphy in the Baoshan area and enabling a more precise correlation with other sections around the world. In total, 19 different forms of P_1 elements, which belong to six different form genera, are found within the *M. bidentata* Zone of lower Sevatian. When these are combined with reported form species in the same conodont zone, a peak in conodont diversification is revealed in the *M. bidentata* Zone. This peak was followed by a distinct decline in conodont diversity and a pronounced morphologic change and turnover in the uppermost *M. bidentata* Zone, which may represent the first crisis of the protracted suite of end-Triassic mass extinctions.

Acknowledgements

We thank Y.F. Gong and Q. Cao for field assistance in sampling. SEM pictures were taken at the State Key Laboratory of Biogeology and Environmental Geology in China University of Geosciences and at the Wuhan Center of Geological Survey. C.B. Yan is appreciated in helping with the SEM photographs. Special thanks to M. Rigo, X.L. Lai and to the reviewers M. Leu, M.L. Golding and V. Karádi for their suggestions on conodont taxonomy, and to editor Kenneth De Baets for his useful comments during review process.

References

Ali, J.R., Cheung, H.M.C., Aitchison, J.C., and Sun, Y., 2013. Palaeomagnetic re-investigation of Early Permian rift basalts from the Baoshan Block, SW China: constraints on the site-of-origin of the Gondwana-derived eastern Cimmerian terranes: Geophysical Journal International, v. 193, p. 650–663. https://doi.org/10.1093/gji/ggt012

Balini, M., Bertinelli, A., Di Stefano, P., Guaiumi, C., Levera, M., Mazza, M., Muttoni, G., Nicora, A., Preto, N., and Rigo, M., 2010. The late Carnian-Rhaetian succession at Pizzo Mondello (Sicani Mountains): Albertiana, v. 39, p. 36–57.

Balini, M., Krystyn, L., Levera, M., and Tripodo, A., 2012. Late Carnian-Early Norian ammonoids from the GSSP candidate section Pizzo Mondello (Sicani Mountains, Sicily): Rivista Italiana di Paleontologia e Stratigrafia, v. 118, p. 47–84. https://doi.org/10.13130/2039-4942/5992

Bambach, R.K., Knoll, A.H., and Wang, S.C., 2004. Origination, extinction, and mass depletions of marine diversity: Paleobiology, v. 30(4), p. 522–542. https://doi.org/10.1666/0094-8373(2004)030<0522:OEAMDO>2.0.CO;2

Baranyi, V., Reichgelt, T., Olsen, P.E., Parker, W.G., and Kürschner, W.M., 2018. Norian vegetation history and related environmental changes: New data from the Chinle Formation, Petrified Forest National Park (Arizona, SW USA): GSA Bulletin, v. 130(5-6), p. 775–795. https://doi.org/10.1130/B31673.1

Bazzucchi, P., Bertinelli, A., Ciarapica, G., Marcucci, M., Passeri, L., Rigo, M., et al., 2005. The Late Triassic-Jurassic stratigraphic succession of Pignola (Lagonegro-Molise Basin, Southern Apennines, Italy: Italian Journal of Geosciences, v. 124(1), p. 143–153.

Benson, R.B.J., Butler, R.J., Lindgren, J., and Smith, A.S., 2009. Mesozoic marine tetrapod diversity: mass extinctions and temporal heterogeneity in geological megabiases affecting vertebrates: Proceedings of the Royal Society B: Biological Sciences, v. 277, p. 829–834. https://doi.org/10.1098/rspb.2009.1845

Benton, M.J., 1986. More than one event in the late Triassic mass extinction: Nature, v. 321, p. 857–861. https://doi.org/10.1038/321857a0

Benton, M.J., 1993. Late Triassic extinctions and the origin of dinosaurs: Science, v. 260, p. 769–771. https://doi.org/10.1126/science.260.5109.7

Benton, M.J., Ruta, M., Dunhill, A.M., and Sakamoto, M., 2013. The first half of tetrapod evolution, sampling proxies, and fossil record quality: Palaeogeography, Palaeoclimatology, Palaeoecology, v. 372, p. 18–41. https://doi.org/10.1016/j.palaeo.2012.09.005

Bertinelli, A., Ciarapica, G., De Zanche, V., Marcucci, M., Passeri, L., Rigo, M., and Roghi, G., 2005. Stratigraphic evolution of the Triassic-Jurassic Sasso di Castalda succession (Lagonegro basin, Southern Apennines, Italy): Italian Journal of Geosciences, v. 124(1), p. 161–175.

Bertinelli, A., Casacci, M., Concheri, G., Gattolin, G., Godfrey, L., Katz, M., Maron, M., Mazza, M., Mietto, P., and Muttoni, G., 2016. The Norian/Rhaetian boundary interval at Pignola-Abriola section (Southern Apennines, Italy) as a GSSP candidate for the Rhaetian Stage: an update: Albertiana, v. 43, p. 5–18.

BGMRY, 1980. Geological Map Sheet Baoshan with Explanation: Bureau of Geology and Mineral Resources of Yunnan Province, scale 1:200,000. [in Chinese]

BGMRY, 1981. Geological Map Sheet Fengqing with Explanation: Bureau of Geology and Mineral Resources of Yunnan Province, scale 1:200,000. [in Chinese]

BGMRY, 1990. Regional Geology of Yunnan province: Geological Publishing House, Beijing, 728 p. [in Chinese]

Budurov, K.J. and Sudar, M.N., 1990. Late Triassic conodont stratigraphy: Courier Forschungsinstitut Senckenberg, v. 118, p. 203–239.

Cai, F., Ding, L., Yao, W., Laskowski, A.K., Xu, Q., Zhang, J.E., and Sein, K., 2017. Provenance and tectonic evolution of Lower Paleozoic–Upper Mesozoic strata from Sibumasu terrane, Myanmar: Gondwana Research, v. 41, p. 325–336. https://doi.org/10.1016/j.gr.2015.03.005

Carter, E.S., and Orchard, M.J., 2007. Radiolarian-conodont-ammonoid intercalibration around the Norian-Rhaetian boundary and implications for trans-Panthalassan correlation: Albertiana, v. 36, p. 149–163.

Channell, J.E.T., Kozur, H.W., Sievers, T., Mock, R., Aubrecht, R., and Sykora, M., 2003. Carnian–Norian biomagnetostratigraphy at Silická Brezová (Slovakia): correlation to other Tethyan sections and to the

Newark Basin: Palaeogeography, Palaeoclimatology, Palaeoecology, v. 191, p. 65–109. https://doi.org/10.1016/S0031-0182(02)006545

Cohen, K.M., Harper, D.A.T., Gibbard, P.L., and Fan, J.X., 2019. ICS International Chronostratigraphic Chart. International Commission on Stratigraphy. https://stratigraphy.org/chart.

Demangel, I., Kovács, Z., Richoz, S., Gardin, S., Krystyn, L., Baldermann, A., and Piller, W. E., 2020. Development of early calcareous nannoplankton in the late Triassic (Northern Calcareous Alps, Austria): Global and Planetary Change, v. 193, p. 103–254. https://doi.org/10.1016/j.gloplacha.2020.103254

Demo, F., 2017. Analysis of synchrotron microtomography 3D images of exceptional fused cluster of *Mockina slovakensis* (Conodonts). Thesis, Università degli Studi di Padova, Italy.

Dong, Z.Z., and Wang, W., 2006. Biostratigraphy and biogeography of conodont fauna in Yunnan, Yunnan Science and Technology Press, 347 p. [in Chinese with English abstract]

Du, Y.X., Bertinelli, A., Jin, X., Shi, Z.Q., Karádi, V., Yin, H., Han, L., Wu, Q.W., Rigo, M., 2020. Integrated conodont and radiolarian biostratigraphy of the upper Norian in Baoshan Block, Southwestern China. Lethaia, v. 53(4), p. 533–545. https://doi.org/10.1111/let.12374

Du, Y.X., Onoue, T., Karádi, V., Williams, I.S., Rigo, M., 2021. Evolutionary Process from *Mockina bidentata* to *Parvigondolella andrusovi*: Evidence from the Pizzo Mondello Section, Sicily, Italy. Journal of Earth Science, v. 32(3), p. 667–676. https://doi.org/10.1007/s12583-020-1362-2

Dzik, J., 1976. Remarks on the evolution of Ordovician conodonts: Acta Palaeontologica Polonica, v. 21, p. 395–455.

Gale, L., Kolar-Jurkovšek, T., Šmuc, A., and Rožič, B., 2012. Integrated Rhaetian foraminiferal and conodont biostratigraphy from the Slovenian Basin, eastern Southern Alps: Swiss Journal of Geosciences, v. 105, p. 435–462. https://doi.org/10.1007/s00015-012-0117-1

Gardin, S., Krystyn, L., Richoz, S., Bartolini, A., and Galbrun, B., 2012. Where and when the earliest coccolithophores?: Lethaia, v. 45(4), p. 507–523. https://doi.org/10.1111/j.1502-3931.2012.00311.x

Gaździcki, A., Kozur, H., and Mock, R., 1979. The Norian-Rhaetian boundary in the light of micropaleontological data: Geologija, v. 22, p. 71–112.

Giordano, N., Rigo, M., Ciarapica, G., and Bertinelli, A., 2010. New biostratigraphical constraints for the Norian/Rhaetian boundary: data from Lagonegro Basin, Southern Apennines, Italy: Lethaia, v. 43, p. 573–586. https://doi.org/10.1111/j.1502-3931.2010.00219.x

Golonka, J., Embry, A., and Krobicki, M., 2018. Late Triassic global plate tectonics, *in* Tanner L. H., ed., The Late Triassic World: Earth in a Time of Transition: Springer, p. 27–57. DOI: 10.1007/978-3-319-68009-5_2

Goudemand, N., Orchard, M.J., Urdy, S., Bucher, H., Tafforeau, P., 2011. Synchrotron-aided reconstruction of the conodont feeding apparatus and implications for the mouth of the first vertebrates: Proceedings of the National Academy of Sciences, v. 108(21), p. 8720–8724. https://doi.org/10.1073/pnas.1101754108

Goudemand, N., Orchard, M.J., Tafforeau, P., Urdy, S., Brühwiler, T., Brayard, A., et al., 2012. Early Triassic conodont clusters from south China: revision of the architecture of the 15 element apparatuses of the superfamily gondolelloidea: Palaeontology, v. 55(5), p. 1021–1034. https://doi.org/10.1111/j.1475-4983.2012.01174.x

Hallam, A., 2002. How catastrophic was the end-Triassic mass extinction?: Lethaia, v. 35, p. 147–157.

Hayashi, S., 1968. The Permian conodonts in chert of the Adoyama Formation, Ashio mountains, central Japan: Earth Science, v. 22, p. 63–77. https://doi.org/10.1111/j.1502-3931.2002.tb00075.x

Hirsch, F., and Ishida, K., 2002. The Izanami Plateau: Pre-accretionary origin of Japan's low-latitude Triassic pelagic carbonates: Eclogae Geologicae Helvetiae, v. 95, p. 43–56.

Hornung T., 2005. Palaeoclimate background and stratigraphic evidence of Late Norian/Early Rhaetian polyphase synsedimentary tectonics in the Hallstatt Limestones of Berchtesgaden (Rappoltstein, Southern Germany): Austrian Journal of Earth Sciences, v. 98, p. 106–119.

Huckriede, R., 1958. Die Conodonten der mediterranen Trias und ihr stratigraphischer Wert: Paläontologische Zeitschrift, v. 32, p. 141–175.

Huang, J.Y., Hu, S.X., Zhang, Q.Y., Donoghue, P.C.J., Benton, M.J., Zhou, C.Y., et al., 2019a. Gondolelloid multielement conodont apparatus (*Nicoraella*) from the Middle Triassic of Yunnan Province, southwestern China: Palaeogeography, Palaeoclimatology, Palaeoecology, v. 522, p. 98–110. https://doi.org/10.1016/j.palaeo.2018.07.015

Huang, J.Y., Martínez-Pérez, C., Hu, S.X., Donoghue, P.C.J., Zhang, Q.Y., Zhou, C.Y., et al., 2019b. Middle Triassic conodont apparatus architecture revealed by synchrotron X-ray microtomography: Palaeoworld, v. 28(4), p. 429–440. https://doi.org/10.1016/j.palwor.2018.08.003

Ishida, K. and Hirsch, F., 2001. Taxonomy and faunal affinity of late Carnian Rhaetian conodonts in the southern Chichibu belt, Shikoku, SW Japan: Rivista Italiana di Paleontologia e Stratigrafia (Research In Paleontology and Stratigraphy), v. 107(2), p. 227–250. https://doi.org/10.13130/2039-4942/5433

Ji, Z.S., Yao, J.X., Yang, X.D., Zang, W.S and Wu, G.C., 2003. Conodont zonations of Norian in Lhasa area, Xizang (Tibet) and their global correlation: Acta Palaeontologica Sinica, v. 42, p. 382–392. [in Chinese with English summary]

Jiang, H.S., Yuan, J.L., Chen, Y., Ogg, J.G., and Yan, J.X., 2019. Synchronous onset of the Mid-Carnian Pluvial Episode in the East and West Tethys: Conodont evidence from Hanwang, Sichuan, South China: Palaeogeography, Palaeoclimatology, Palaeoecology, v. 520, p. 173–180. https://doi.org/10.1016/j.palaeo.2019.02.004

Jin, X., Du, Y.X., Bertineli, A., Shi, Z.Q., Preto, N., Zou, H., Ogg, J.G., Han, L., Wu, Q.W. and Rigo, M., 2022. Carbon-isotope excursions in the Norian stage (Upper Triassic) of the Baoshan terrane, western Yunnan, China. Journal of Asian Earth Sciences, v. 230, 105215. https://doi.org/10.1016/j.jseaes.2022.105215

Karádi, V, 2018. Middle Norian conodonts from the Buda Hills, Hungary: an exceptional record from the western Tethys: Journal of Iberian Geology, v. 44, p. 155–174. https://doi.org/10.1007/s41513-017-0009-3

Karádi, V., 2021. Evolutionary trends of the genus *Ancyrogondolella* (Conodonta) and related taxa in the Norian (Late Triassic): Journal of Earth Science, v. 32(3), p. 700–1708. https://doi.org/10.1007/s12583-020-1381-z

Karádi, V., Cau, A., Mazza, M., and Rigo, M., 2020. The last phase of conodont evolution during the Late Triassic: Integrating biostratigraphic and phylogenetic approaches: Palaeogeography, Palaeoclimatology, Palaeoecology, v. 549, n. 109144. https://doi.org/10.1016/j.palaeo.2019.03.045

Karádi, V., Kolar-Jurkovšek, T., Gale, L., and Jurkovšek, B., 2021. New Advances in Biostratigraphy of the Lower/Middle Norian Transition: Conodonts of the Dovško Section, Slovenia: Journal of Earth Science, v. 32(3), p. 677–699. https://doi.org/10.1007/s12583-020-1382-y

Karádi, V., Pelikán, P., and Haas, J., 2016. A Budai-hegység felső-triász medence kifejlődésű dolomitjainak conodonta biosztratigráfiája: Földtani Közlöny, v. 146(4), p. 371–386.

Kent, D.V., Olsen, P.E., and Muttoni, G., 2017. Astrochronostratigraphic polarity time scale (APTS) for the Late Triassic and Early Jurassic from continental sediments and correlation with standard marine stages. Earth-Science Reviews, v. 166, p. 153–180. https://doi.org/10.1016/j.earscirev.2016.12.014

Korte, C., Kozur, H.W., and Veizer, J., 2005. $\delta^{13}C$ and $\delta^{18}O$ values of Triassic brachiopods and carbonate rocks as proxies for coeval seawater and palaeotemperature: Palaeogeography, Palaeoclimatology, Palaeoecology, v. 226, p. 287–306. https://doi.org/10.1016/j.palaeo.2005.05.018

Kovács, S., and Kozur, H., 1980. Stratigraphische Reichweite der wichtigsten conodonten (ohne Zahnreihenconodonten) der Mittel-und Obertrias: Geologisch-Paläontologische Mitteilungen Innsbruck, v. 10, p. 47–78.

Kovács, S., and Nagy, G., 1989. Contributions to the age of the Avicula- and Halobia-limestones (Fekete-hegy Limestone Formation) in Pilis Mts (NE Transdanubian Central Range, Hungary): Annual Report of the Hungarian Geological Institute, 1987, p. 95–129. [in Hungarian with English summary]

Kozur, H., 1972. Die Conodontengattung Metapolygnathus Hayashi 1968 und ihr stratigraphischer: Wart. Geol. Paleontol. Mitt. Innsbruck, v. 2, p. 1–37.

Kozur, H., 1973. Beiträge zur Stratigraphie und Paläontologie der Trias: Geologisch-Paläontologische Mitteilungen Innsbruck, v. 1, p. 1–30.

Kozur, H., 1990. The taxonomy of the gondolellid conodonts in the Permian and Triassic: Courier Forschungs Institut Senckenberg, v. 117, p. 409–469.

Kozur, H., 2003. Integrated ammonoid, conodont and radiolarian zonation of the Triassic and some remarks to stage/substage subdivision and the numeric age of the Triassic stages: Albertiana, v. 28, p. 57–74.

Kozur, H., and Mock, R., 1972. Neue Conodonten aus der Trias der Slowakei und ihre stratigraphische Bedeutung: Geologisch-Paläontologische Mitteilungen Innsbruck, v. 2, p. 1–20.

Kozur, H., and Mock, R., 1974. Zwei neue Conodonten-Arten aus der Trias des slowakischen Karstes: Časopis Min. Geol. Roc, v. 19, p. 135–139.
Kozur, H., and Mock, R., 1991. New Middle Carnian and Rhaetian conodonts from Hungary and the Alps. Stratigraphic importance and tectonic implications for the Buda Mountains and adjacent areas: Jahrbuch der geologischen Bundesanstalt, v. 134, p. 271–297.
Kozur, H., and Mostler, H, 1971. Probleme der Conodontenforschung in der Trias: Geologisch-Paläontologische Mitteilungen Innsbruck, v. 4, p. 1–19.
Kozur, H., and Mostler, H., 1972. Die Bedeutung der Conodonten für stratigraphische und paläogeographische Untersuchungen in der Trias: Mitt. Ges. Geol. Bergbaustud, v. 21, p. 777–810.
Krystyn, L., 1980. Triassic conodont localities of the Salzkammergut region: Abh. Geol. BA, v. 35, p. 61–98.
Krystyn, L., Bouquerel, H., Kürschner, W., Gallet, S., and Richoz, A., 2007. Proposal for a candidate GSSP of the base of the Rhaetian Stage, *in* Lucas, S.G. and Spielmann, J.A., eds., The Global Triassic. New Mexico Museum of Natural History and Science Bulletin, v. 41, p. 189–199.
Li, D.Y., 1976. The Triassic of Yunnan, Yunnan Institute of Geological Sciences, v. 2, p. 342–353. [in Chinese]
Liao, S.Y., Wang, D.B., Tang, Y., Yin, F.G., Cao, S.N., Wang, L.Q., Wang, B.D., and Sun, Z.M., 2015. Late Paleozoic Woniusi basaltic province from Sibumasu terrane: Implications for the breakup of eastern Gondwana's northern margin: Geological Society of America Bulletin, v. 127, p. 1313–1330. https://doi.org/10.1130/B31210.1
Lindström, M., 1970, A suprageneric taxonomy of the conodonts: Lethaia, v. 4, p. 427–445. https://doi.org/10.1111/j.1502-3931.1970.tb00834.x
Lucas, S.G., 2018. Late Triassic ammonoids: Distribution, biostratigraphy and biotic events, *in* Tanner L. H., ed., The Late Triassic World: Earth in a Time of Transition: Springer, p. 237–261. https://doi.org/10.1007/978-3-319-68009-5_7
Lucas, S.G., 2021. End-Triassic Extinctions, *in* David, A., and Scott A.E., Encyclopedia of Geology (second edition): Oxford Academic Press, p. 653–664.
Lucas, S.G., and Tanner, L.H., 2008. Reexamination of the end-Triassic mass, Mass extinction: Springer, Berlin, Heidelberg, p. 65–102. https://doi.org/10.1007/978-3-540-75916-4_8
Lucas, S.G., and Tanner, L.H., 2015. End-Triassic nonmarine biotic events: Journal of palaeogeography, v. 4(4), p. 331–348. https://doi.org/10.1016/j.jop.2015.08.010
Mader, A.F., 2015. Record of climatic changes in the Triassic palynological spectra from Poland: Geological Quarterly, v. 59(4), p. 615–653. DOI: https://doi.org/10.7306/gq.1239
Mao, L., and Tian, C.R., 1987. Late Triassic conodonts from the uppermost Mailonggang Formation in Mailonggang village of Lhünzhub County, Xizang (Tibet), China: Bulletin of the Chinese Academy of Geological Sciences, v. 17, p. 159–168. [in Chinese with English summary]
Martínez-Pérez, C., Cascales-Miñana, B., Plasencia, P., and Botella, H., 2015. Exploring the major depletions of conodont diversity during the Triassic: Historical Biology, v. 27, p. 503–507. https://doi.org/10.1080/08912963.2014.890192
Martini, R., Zaninetti, L., Villeneuve, M., Cornee, J.-J., Krystyn, L., Cirilli, S., De Wever, P., Dumitrica, P., and Harsolumakso, A., 2000. Triassic pelagic deposits of Timor: palaeogeographic and sea-level implications: Palaeogeography, Palaeoclimatology, Palaeoecology, v. 160, p. 123–151. https://doi.org/10.1016/S0031-0182(00)00062-6
Mazza, M., Rigo, M., and Gullo, M., 2012. Taxonomy and biostratigraphic record of the Upper Triassic conodonts of the Pizzo Mondello section (western Sicily, Italy), GSSP candidate for the base of the Norian: Rivista Italian di Paleontologia e Stratigrafia, v. 118, p. 85–130.
McRoberts, C.A., 2010. Biochronology of Triassic bivalves. Geological Society, London, Special Publications, v. 334(1), p. 201–219. https://doi.org/10.1144/SP334.9
McRoberts, C.A., Krystyn, L., and Shea, A., 2008. Rhaetian (Late Triassic) *Monotis* (Bivalvia: Pectinoida) from the eastern Northern Calcareous Alps (Austria) and the end-Norian crisis in pelagic faunas: Palaeontology, v. 51, p. 721–735. https://doi.org/10.1111/j.1475-4983.2008.00776.x
Meek, R.H., 1984. Conodonts from the Norian (Upper Triassic) basin and shelf facies, northwestern Nevada: Conodont biofacies and provincialism: Geological Society of America Special Paper, v. 196, p. 307–324.

Moix, P., Kozur, H.W., Stampfli, G.M., and Mostler, H., 2007. New paleontological, biostratigraphical and paleogeographic results from the Triassic of the Mersin Mélange, SE Turkey, *in* Lucas, S.G. and Spielmann, J.A., eds., The Global Triassic: New Mexico Museum of Natural History and Science Bulletin, v. 41, p. 282–311.

Morley, C.K., 2018. Understanding Sibumasu in the context of ribbon continents: Gondwana Research, v. 64, p. 184–215. https://doi.org/10.1016/j.gr.2018.07.006

Mosher, L.C., 1968. Triassic conodonts from western North America and Europe and their correlation: Journal of Paleontology, v. 42, p. 895–946.

Muttoni, G., Mazza, M., Mosher, D., Katz, M.E., Kent, D.V., and Balini, M., 2014. A Middle–Late Triassic (Ladinian–Rhaetian) carbon and oxygen isotope record from the Tethyan Ocean: Palaeogeography, Palaeoclimatology, Palaeoecology, v. 399, p. 246–259. https://doi.org/10.1016/j.palaeo.2014.01.018

Onoue, T., Sato, H., Yamashita, D., Ikehara, M., Yasukawa, K., Fujinaga, K., Kato, Y., and Matsuoka, A., 2016. Bolide impact triggered the Late Triassic extinction event in equatorial Panthalassa: Scientific Reports, v. 6, p. 296–309. https://doi.org/10.1038/srep29609

Onoue, T., Hori, R.S., and Kojima, S., 2017. Triassic and Jurassic radiolarian response to global catastrophic events in the Panthalassa Ocean, as recorded in the Mino Belt, central Japan: Science Reports of Niigata University (Geology), v. 32, p. 59–69.

Onoue, T., Yamashita, K., Fukuda, C., Soda, K., Tomimatsu, Y., Abate, B., and Rigo, M., 2018. Sr isotope variations in the Upper Triassic succession at Pizzo Mondello, Sicily: Constraints on the timing of the Cimmerian Orogeny: Palaeogeography, Palaeoclimatology, Palaeoecology, v. 499, p. 131–137. https://doi.org/10.1016/j.palaeo.2018.03.025

Orchard, M.J., 1983. *Epigondolella* populations and their phylogeny and zonation in the Upper Triassic: Fossils and Strata, v. 15, p. 177–192.

Orchard, M.J., 1991a. Late Triassic conodont biochronology and biostratigraphy of the Kunga Group, Queen Charlotte Islands, British Columbia, *in* Woodsworth, G.J., ed., Evolution and Hydrocarbon potential of Queen Charlotte Basin, British Columbia: Geol. Surv. Canad, p. 173–193.

Orchard, M.J., 1991b. Upper Triassic conodont biochronology and new index species from the Canadian Cordillera, *in* Orchard, M.J. and McCracken, A.D., eds., Ordovician to Triassic conodont paleontology of the Canadian Cordillera: Geological Survey of Canada, Vancouver, v. 417, p. 299–335.

Orchard, M.J., 2005. Multielement conodont apparatuses of Triassic Gondolelloidea, *in* Purnell, M.A., and Donoghe, P.C.J. eds., Conodont Biology and Phylogeny: Interpreting the Fossil Record: Special Papers in Palaeontology, v. 73, p. 73–101.

Orchard, M.J., 2018. The Lower-Middle Norian (Upper Triassic) boundary: New conodont taxa and a refined biozonation: Bulletins of American Paleontology, v. 395–396, p. 165–193.

Orchard, M.J., Whalen, P.A., Carter, E.S., and Taylor, H., 2007a. Latest Triassic conodonts and radiolarian-bearing successions in Baja California Sur, *in* Lucas, S.G. and Spielmann, J.A., eds., The Global Triassic. New Mexico Museum of Natural History and Science Bulletin, v. 41, p. 355–365.

Orchard, M.J., Carter, E.S., Lucas, S.G., and Taylor, D., 2007b. Rhaetian (Upper Triassic) conodonts and radiolarians: Albertiana, v. 35, p. 59–65.

Pálfy, J., Demény, A., Haas, J., Carter, E.S., Görög, Á., Halász, D., Oravecz-Scheffer, A., Hetényi, M., Márton, E., and Orchard, M.J., 2007. Triassic–Jurassic boundary events inferred from integrated stratigraphy of the Csővár section, Hungary: Palaeogeography, Palaeoclimatology, Palaeoecology, v. 244, p. 11–33. https://doi.org/10.1016/j.palaeo.2006.06.021

Pander, C.H., 1856. Monographie der fossilen Fische des silurischen Systems der russisch-baltischen Gouvernements: Akademie der Wissenschaften, St. Petersburg, 91 p.

Plasencia, P., Aliaga, A.M., and Sha, J.G., 2013. A database of Triassic conodonts from a comprehensive revision of literature: Revista Española de Paleontología, v. 28, p. 215–226.

Racki, G., and Lucas, S.G., 2020. Timing of dicynodont extinction in light of an unusual Late Triassic Polish fauna and Cuvier's approach to extinction: Historical Biology, v. 32(4), p. 452–461. https://doi.org/10.1080/08912963.2018.1499734

Rigo, M., De Zanche, V., Gianolla, P., Mietto, P., Preto, N., and Roghi, G., 2005. Correlation of Upper Triassic sections throughout the Lagonegro Basin: Bollettino Società Geologica Italiana, v. 124, p. 293–300.

Rigo, M., Bertinelli, A., Concheri, G., Gattolin, G., Godfrey, L., Katz, M.E., Maron, M., Mietto, P., Muttoni, G., and Sprovieri, M., 2016. The Pignola-Abriola section (southern Apennines, Italy): a new GSSP candidate for the base of the Rhaetian Stage: Lethaia, v. 49, p. 287–306. https://doi.org/10.1111/let.12145

Rigo, M., Mazza, M., Karádi, V., and Nicora, A., 2018. New Upper Triassic conodont biozonation of the Tethyan Realm, *in* Tanner L. H., ed., The Late Triassic World: Earth in a Time of Transition: Springer, p. 189–235. https://doi.org/10.1007/978-3-319-68009-5

Rigo, M., Onoue, T., Tanner, L.H., Lucas, S.G., Godfrey, L., Katz, M.E., Zaffani, M., Grice, K., Cesar, J., Yamashita, D., Maron, M., Tackett, L.S., Campbel, H., Tateo, F., Concheri, G., Agnini, C., Chiari, M., and Bertinelli, A., 2020. The Late Triassic Extinction at the Norian/Rhaetian boundary: Biotic evidence and geochemical signature: Earth-Science Reviews, v. 204, p. 103-180. https://doi.org/10.1016/j.earscirev.2020.103180

Rožič, B., Kolar-Jurkovšek, T., and Šmuc, A., 2009. Late Triassic sedimentary evolution of Slovenian Basin (eastern Southern Alps): description and correlation of the Slatnik Formation: Facies, v. 55, p. 137-155. https://doi.org/10.1007/s10347-008-0164-2

Sephton, M.A., Amor, K., Franchi, I.A., Wignall, P.B., Newton, R., and Zonneveld, J.P., 2002. Carbon and nitrogen isotope disturbances and an end-Norian (Late Triassic) extinction event: Geology, v. 30, p. 1119–1122. https://doi.org/10.1130/0091-7613(2002)030<1119:CANIDA>2.0.CO;2

Sone, M., and Metcalfe, I., 2008. Parallel Tethyan sutures in mainland Southeast Asia: New insights for Palaeo-Tethys closure and implications for the Indosinian orogeny: Comptes Rendus Geosciences, v. 340, p. 166–179. https://doi.org/10.1016/j.crte.2007.09.008

Sato, H., Ishikawa, A., Onoue, T., Tomimatsu, Y. and Rigo, M., 2021. Sedimentary record of Upper Triassic impact in the Lagonegro Basin, southern Italy: Insights from highly siderophile elements and Re-Os isotope stratigraphy across the Norian/Rhaetian boundary: Chemical Geology, v. 586, 120506. https://doi.org/10.1016/j.chemgeo.2021.120506

Tanner, L.H., Lucas, S.G., and Chapman, M.G., 2004. Assessing the record and causes of Late Triassic extinctions: Earth-Science Reviews, v. 65, p. 103–139. https://doi.org/10.1016/S0012-8252(03)00082-5

Tian, C.R., 1982. Triassic conodonts in the Tulong section from Nyalam county, *in* Anthology of Tibet Geology: Beijing Geological Publishing House, v. 5, p. 153–165. [in Chinese with English summary]

Trotter, J.A., Williams, I.S., Nicora, A., Mazza, M., and Rigo, M., 2015. Long-term cycles of Triassic climate change: a new $\delta^{18}O$ record from conodont apatite: Earth and Planetary Science Letters, v. 415, p. 165–174. https://doi.org/10.1016/j.epsl.2015.01.038

Vrielynck, B., 1987. Conodontes du Trias périméditerranéen: Systématique, Stratigraphie, *in* Documents des Laboratoires de Géologie Lyon, v. 97, p. 3–306.

Wang, C.Y., and Wang, Z.H., 1976. Triassic conodonts from Mt. Qomolangma (Everest) region, *in* Tibetan Scientific Expedition Team of Chinese Academy of Sciences., ed. Report of scientific expedition in Mt. Qomolangma (Everest) region (Paleontology): Science Press, Beijing, v. 2, p. 387–424. [in Chinese]

Wang, C.Y., and Wang, Z.H., 2016. Conodont Biostratigraphy in China: Hanzhou, Zhejiang, Zhejiang University Press, 379 p. [in Chinese]

Wang, C.Y., Kang, B.X., and Zhang, H.R., 1986. A discovery of Triassic conodonts in the Nadanhada Range and geological significance: Geologic Publishing House, Beijing, China, 109–214 p. [in Chinese with English summary]

Wang, L.J., 1993. The Norian Conodonts of Late Triassic from Western Sichuan and Eastern Xizang: Qinghai Geology, v. 1, p. 24–30, 57–58. [in Chinese with English summary]

Wang, X.D., Du, Y., Shi, Z.Q., and Chen, B., 2019. Characteristics of conodonts and sedimentary environment of upper Norian Nanshuba and Dashuitang Formations in Baoshan, Yunnan province: Acta Palaeontologica Sinica, v. 58, p. 79–91. [in Chinese with English summary]

Wang, Y.Z., Li, X.L., and Duan, L.L., 2000. Tectonic and Mineralization of the Southern Section of the Sanjiang Area: Geological Publishing House, Beijing, p. 1–123. [in Chinese]

Wang, Z.H., and Dong, Z.Z., 1985. Discovery of conodont *Epigondolella* fauna from Late Triassic in Baoshan area, western Yunnan: Acta Micropalaeontologica Sinica, v. 2, p. 125–132. [in Chinese with English summary]

Wang, Z.H., and Wang, L.J., 1990. Several species of the Middle and Late Triassic conodonts from Yushu, Qinghai, *in* Devonian-Triassic Stratigraphy and Palaeontology from Yushu Region of Qinghai, China, Part I: Nanjing University Press, p. 123–129. [in Chinese with English summary]

Ward, P.D., Haggart, J.W., Carter, E.S., Wilbur, D., Tipper, H.W., and Evans, T., 2001. Sudden productivity collapse associated with the Triassic-Jurassic boundary mass extinction: Science, v. 292, p. 1148–1151. https://doi.org/10.1126/science.1058574

Ward, P.D., Garrison, G.H., Haggart, J.W., Kring, D.A., and Beattie, M.J., 2004. Isotopic evidence bearing on Late Triassic extinction events, Queen Charlotte Islands, British Columbia, and implications for the duration and cause of the Triassic/Jurassic mass extinction: Earth and Planetary Science Letters, v. 224(3–4), p. 589–600. https://doi.org/10.1016/j.epsl.2004.04.034

Wiedmann, J., and Kullmann, J., 1996. Crises in ammonoid evolution, *in* Landman, N.H., Tanabe, K., Davis, R.A., eds., Ammonoid paleobiology: Springer, Boston, Ma, p. 795–813. https://doi.org/10.1007/978-1-4757-9153-2_19

Wignall, P.B., Zonneveld, J.P., Newton, R.J., Amor, K., Sephton, M.A., and Hartley, S., 2007. The end Triassic mass extinction record of Williston Lake, British Columbia: Palaeogeography, Palaeoclimatology, Palaeoecology, v. 253, p. 385–406. https://doi.org/10.1016/j.palaeo.2007.06.020

Wignall, P.B., and Atkinson, J.W., 2020. A two-phase end-Triassic mass extinction: Earth-Science Reviews, v. 208, 103282. https://doi.org/10.1016/j.earscirev.2020.103282

Yamashita, D., Kato, H., Onoue, T., and Suzuki, N., 2018. Integrated Upper Triassic conodont and radiolarian biostratigraphies of the Panthalassa Ocean: Paleontological Research, v. 22, p. 167–198. https://doi.org/10.2517/2017PR020

Yuan, J.L., Jiang, H.S., and Wang, D.C., 2015. LST: A new inorganic heavy liquid used in conodont separation: Geological Science and Technology Information, v. 34, p. 225–230. [in Chinese with English summary]

Zhao, Y.J., Zheng, C., Huang, L., Bao, J.F, Li, B., Wang, X.L., and Liu, X.Y., 2012. Catastrophic event characteristics of stratigraphic slope slumping accumulation: a case study of the Upper Triassic Nanshuba Formation in Baoshan area, western Yunnan Province: Geological Bulletin of China, v. 31, p. 745–757. [in Chinese with English summary]

Zeng, W.P., Purnell, M.A., Jiang, H.S., and Zhang, M.H., 2021. Late Triassic (Norian) Conodont Apparatuses Revealed by Conodont Clusters from Yunnan Province, Southwestern China: Journal of Earth Science, v. 32(3), p. 709–724. https://doi.org/10.1007/s12583-021-1459-2

Zhang, M.H., Jiang, H.S., Purnell, M.A., and Lai, X.L., 2017. Testing hypotheses of element loss and instability in the apparatus composition of complex conodonts: articulated skeletons of *Hindeodus*: Palaeontology, v. 60(4), p. 595–608. https://doi.org/10.1111/pala.12305

Figure 1

Geographic locations of the studied sections.

(**A**) Paleogeographic map (after Golonka et al., 2018) showing the position of the Baoshan block during Late Triassic prior to accretion to South China. (**B**) Late Triassic paleogeography map of Yunnan in modern coordinates (modified from BGMRY, 1990) showing the position and the depositional facies of the Baoshan block. (**C**) Map showing the locations of the described sections.

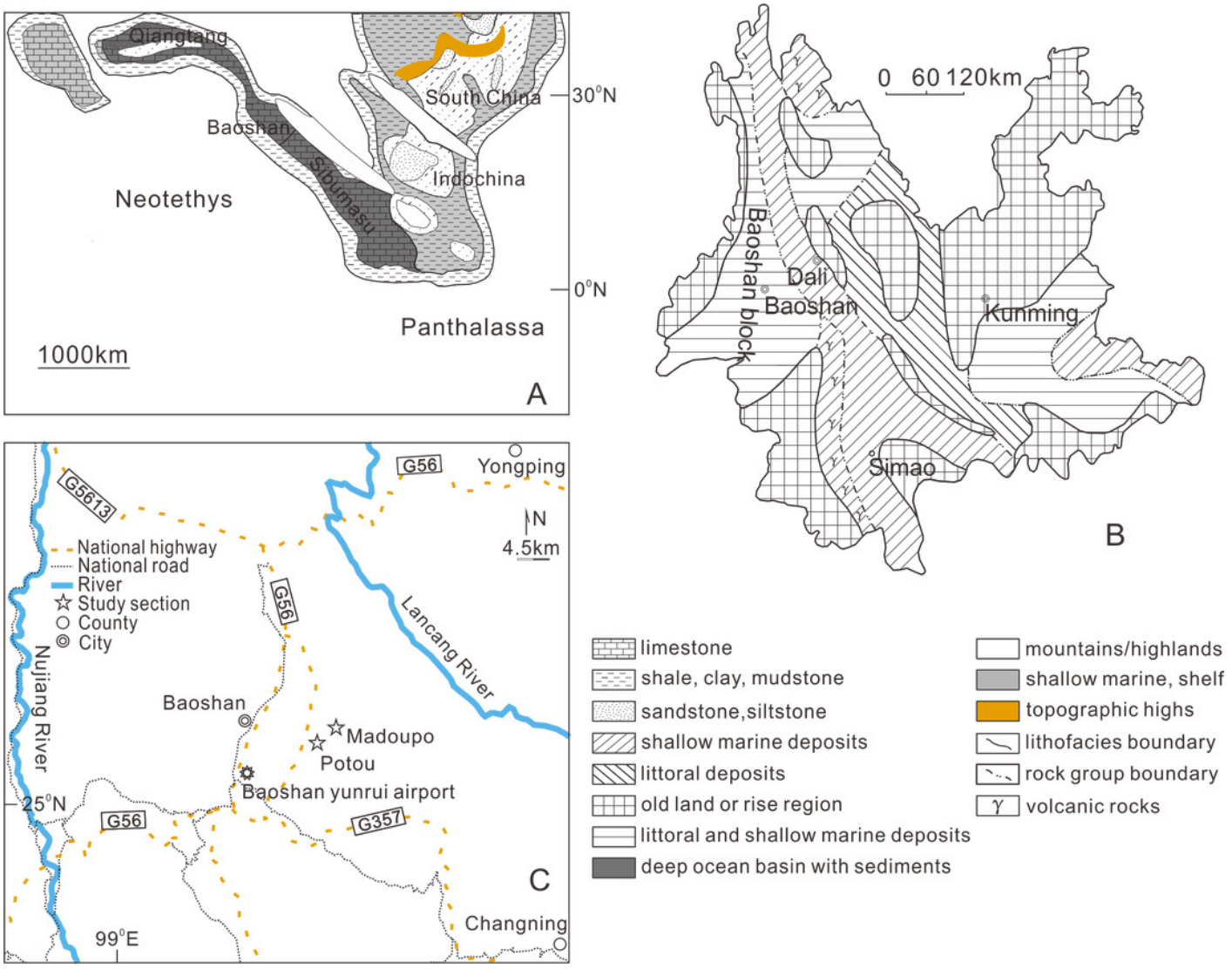

Figure 2

Conodont distribution in the Potou section and in the Madoupo section, Baoshan city, Yunnan Province, southwestern China.

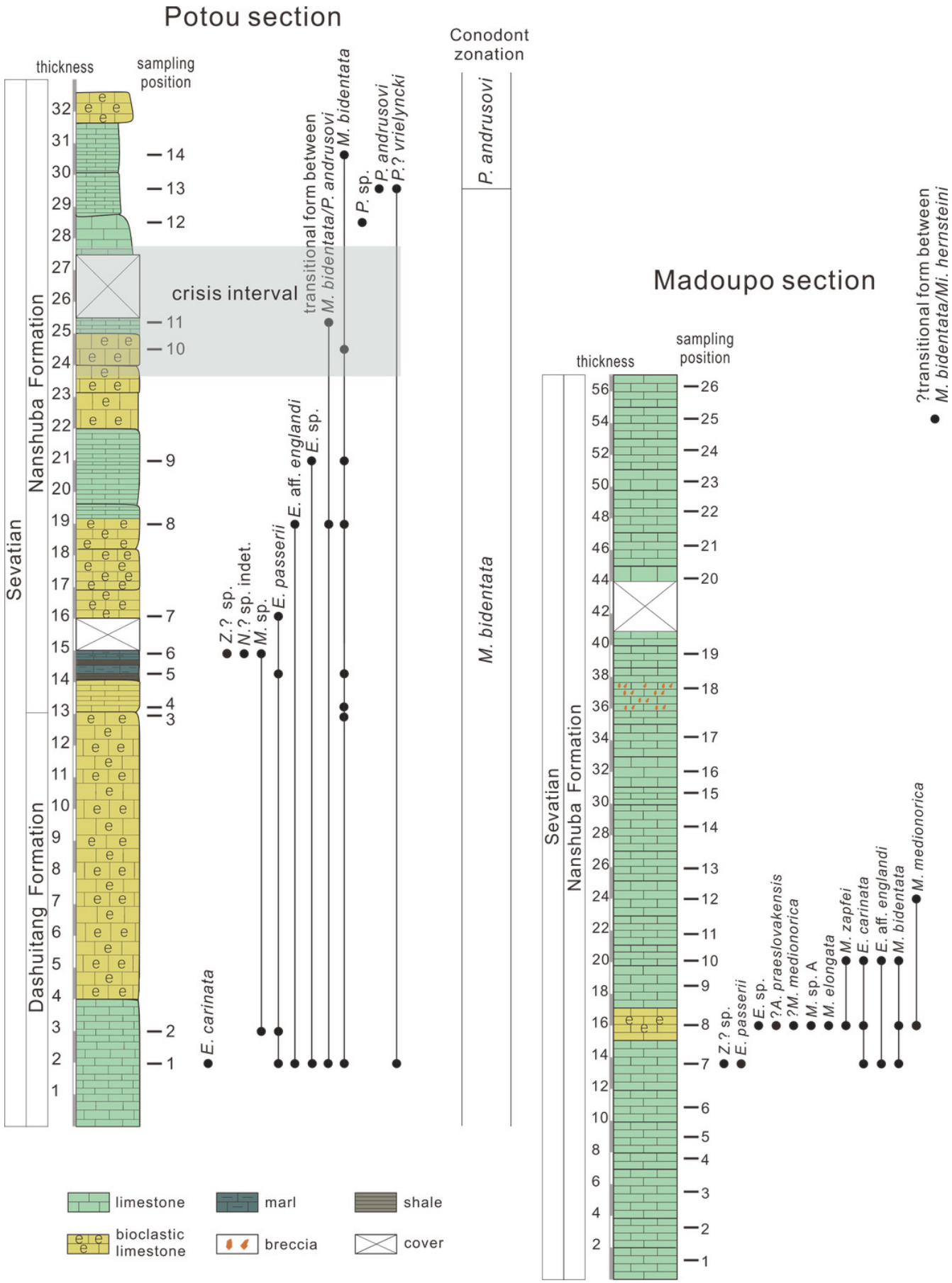
Potou section
thickness
sampling position
Conodont zonation
Sevatian
Nanshuba Formation
Dashuitang Formation
crisis interval
transitional form between M. bidentata/P. andrusovi
M. bidentata
P. sp.
P. andrusovi
P.? vrielyncki
E. aff. englandi
E. sp.
Z.? sp.
N.? sp. indet.
M. sp.
E. passerii
E. carinata
P. andrusovi
M. bidentata
Madoupo section
?transitional form between M. bidentata/Mi. hernsteini
Z.? sp.
E. passerii
E. sp.
?A. praeslovakensis
?M. medionorica
M. sp. A
M. elongata
M. zapfei
E. carinata
E. aff. englandi
M. bidentata
M. medionorica
limestone
marl
shale
bioclastic limestone
breccia
cover

Figure 3

SEM images of conodonts from the Potou section and the Madoupo section.

(**A–T**) *Epigondolella carinata* Orchard, 1991b; A–C, D–F, I–K, L–N, O–Q, catalog nos. are MDP7-038, MDP8-025, MDP7-113, MDP7_i117and MDP10-059, respectively, all from the Nanshuba Formation; G–H, R–T, catalog nos. are POT1_i105 and POT1_i022, respectively, both from the Dashuitang Formation. (**U–BB**) *Epigondolella* sp.; U–W, POT1_i011, from the Dashuitang Formation; X–Z, MDP8_i059, from the Nanshuba Formation; AA–BB, POT9_i050, from the Nanshuba Formation. (**CC–FF, JJ–LL**) *Mockina* sp.; CC, JJ–LL, catalog nos. are POT2-57 and POT2_i058, respectively, all from the Dashuitang Formation; DD–FF, POT6-32, from the Nanshuba Formation. (**GG–II**) ?*Mockina bidentata* (Mosher, 1968), POT9-48, from the Dashuitang Formation. (**MM–OO**) ?*Ancyrogondolella praeslovakensis* (Kozur, Masset and Moix, 2007), MDP8-001, from the Nanshuba Formation. (**PP–QQ**) *Norigondolella*? sp. indet., POT6_i033, from the Nanshuba Formation. (**RR–SS**) *Mockina zapfei* (Kozur, 1973), a juvenile specimen, MDP8-2204, from the Nanshuba Formation. MDP and POT is the abbreviation of Madoupo and Potou, respectively, indicating the specimens come from the two sections respectively.

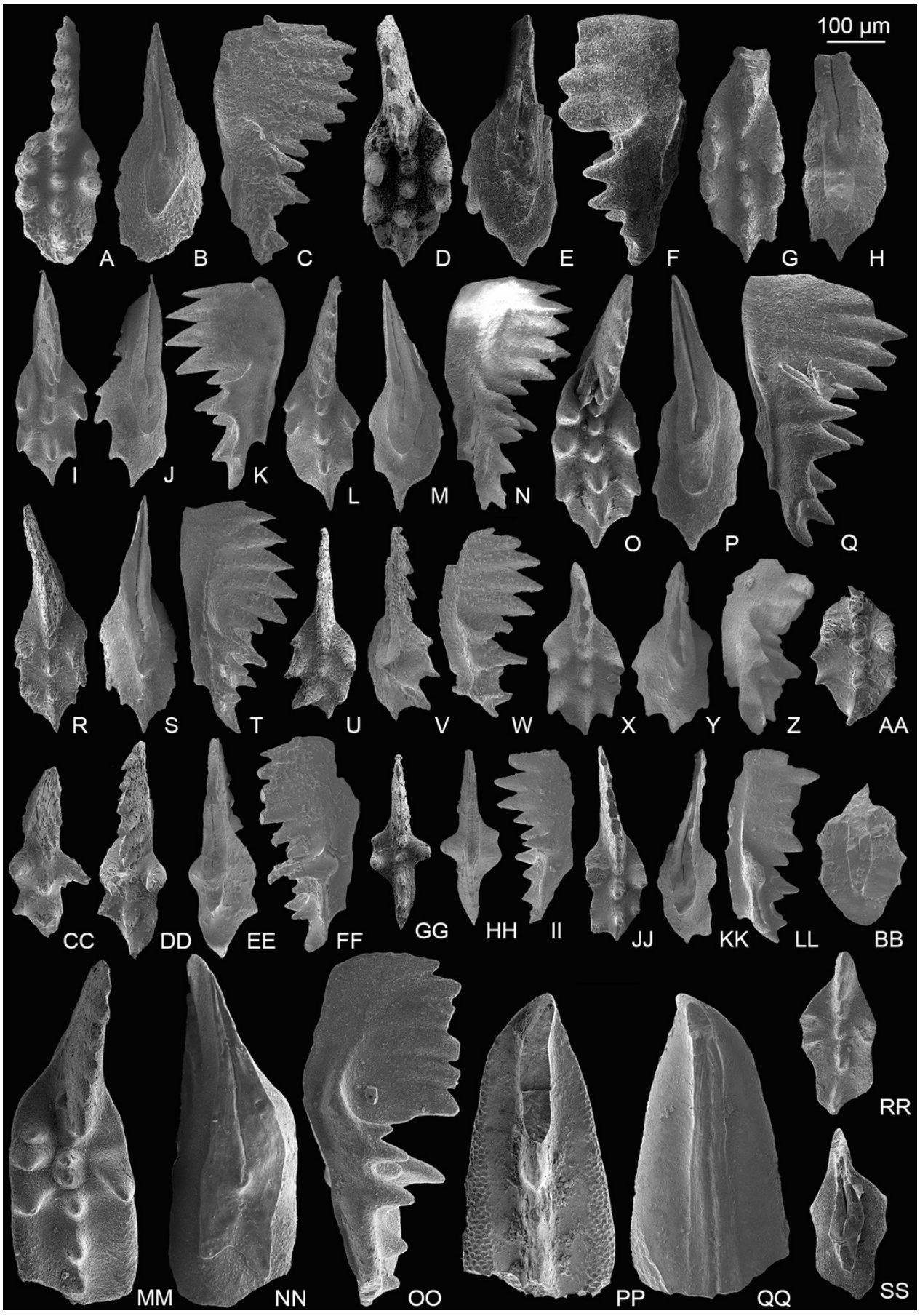
100 µm
A
B
C
D
E
F
G
H
I
J
K
L
M
N
O
P
Q
R
S
T
U
V
W
X
Y
Z
AA
CC
DD
EE
FF
GG
HH
II
JJ
KK
LL
BB
RR
MM
NN
OO
PP
QQ
SS

Figure 4

SEM images of conodonts from the Potou section and the Madoupo section.

(**A–S**) *Epigondolella passerii* (Rigo and Du, 2022); A–C, POT7_i100, from the Nanshuba Formation of the Potou section; D–F, G–I, J–L, M–N, O–P, catalog nos. are POT1_i104, POT2_i097, POT1_i102, POT5_i098 and POT1_i014, respectively, all from the Dashuitang Formation of the Potou section; Q, R–S, catalog nos. are MDP7-3503 and MDP7-3301, respectively, from the Nanshuba Formation of the Madoupo section. (**T–W**) *Zieglericonus*? sp., from the Nanshuba Formation; T–U, MDP7-110, from the Madoupo section; V–W, POT6_i034, from the Potou section. **(X–LL)** *Epigondolella* aff. *englandi* Orchard, 1991b; X–Y, Z–AA, DD–FF and JJ–LL, catalog nos. are POT1_i008, POT1_i020, POT1_i060 and POT1_i009, respectively, all from the Dashuitang Formation of the Potou section; BB–CC, MDP10-061, from the Nanshuba Formation of the Madoupo section; GG–II, POT8_i036, from the Nanshuba Formation of the Potou section.

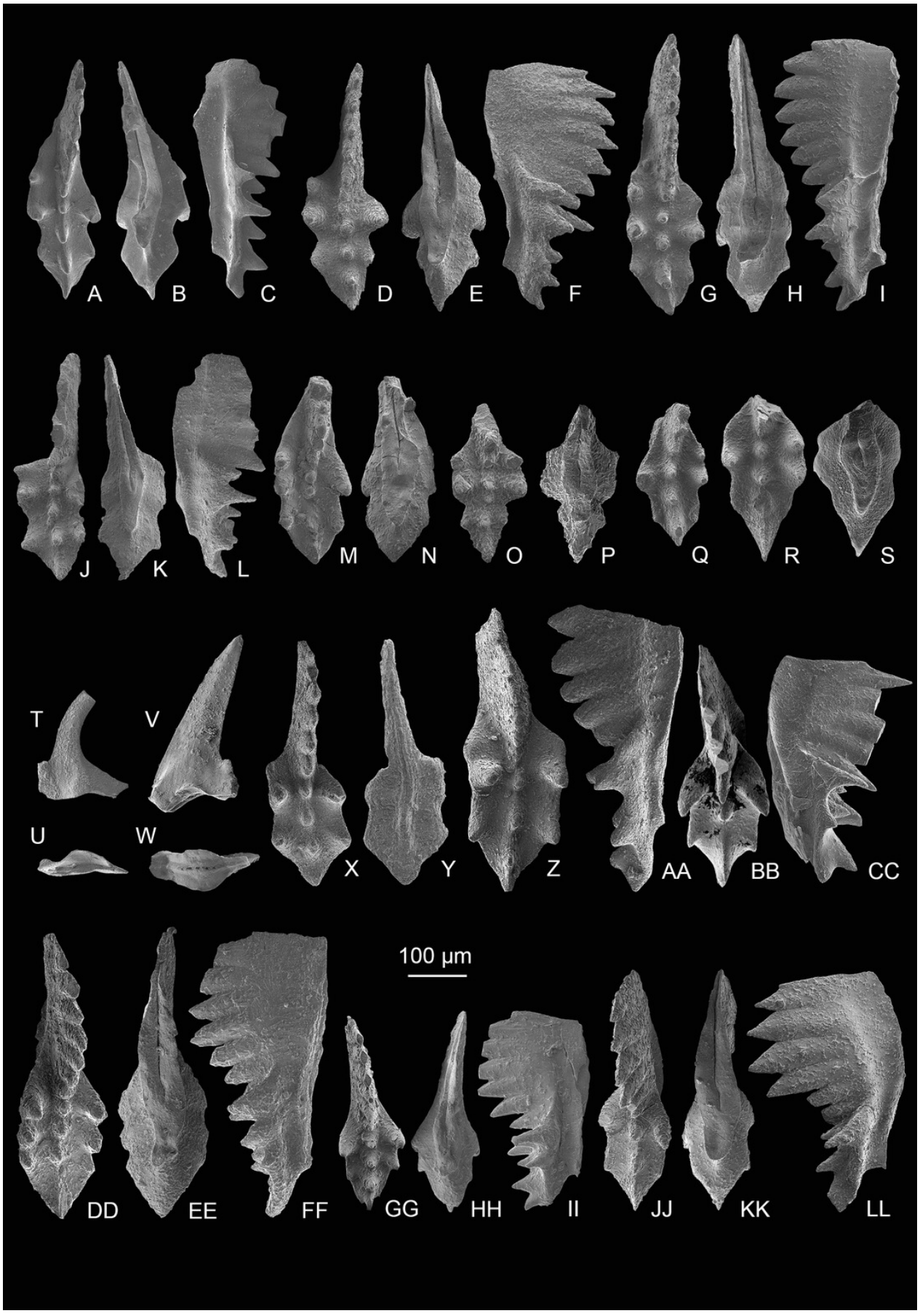
A
B
C
D
E
F
G
H
I
J
K
L
M
N
O
P
Q
R
S
T
V
U
W
X
Y
Z
AA
BB
CC
100 µm
DD
EE
FF
GG
HH
II
JJ
KK
LL

Figure 5

SEM images of conodonts from the Nanshuba Formation of the Madoupo section.

(**A–X**) *Mockina elongata* (Orchard, 1991b); A–C, D–F, G–H, I, J–L, M–N, P–R, S–U, V–X, catalog nos. are MDP8_i053, MDP8_i060, MDP8_i058, MDP8_i036, MDP8_i045, MDP8_i051 (early juvenile specimen), MDP8_i049 (late juvenile specimen), MDP8_i048 and MDP8_i041, respectively. (**Y–BB**) *Mockina medionorica* Kozur, 2003; Y–Z, AA–BB, catalog nos. are MDP12-i118 and MDP8-i039, respectively. **(CC–EE**) *Epigondolella* aff. *englandi* Orchard, 1991b, a juvenile specimen, MDP7-112. **(FF–II)** *Mockina bidentata* (Mosher, 1968); FF–HH, II, catalog nos. are MDP7-3902 and MDP10-060, respectively.

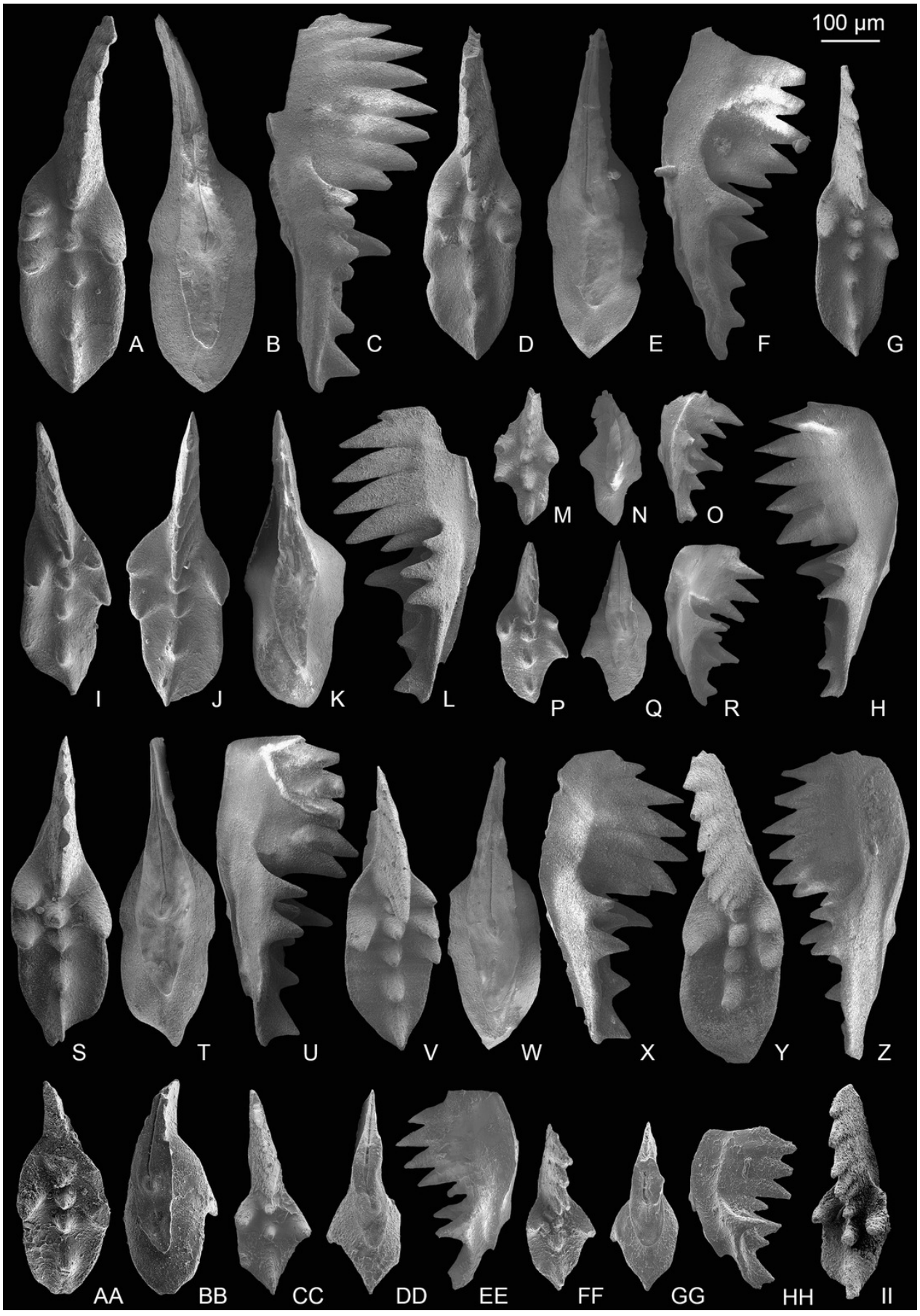
100 µm
A
B
C
D
E
F
G
I
J
K
L
M
N
O
P
Q
R
H
S
T
U
V
W
X
Y
Z
AA
BB
CC
DD
EE
FF
GG
HH
II

Figure 6

SEM images of conodonts from the Potou section and the Madoupo section.

(**A–JJ, DDD**) *Mockina bidentata* (Mosher, 1968); A–B, C**–**E, E–F, G–H, I–K, L–M, N–O, P–Q, R–S, T–U, V, II–JJ, catalog nos. are POT1_i006, POT1_i007, POT1_i018, POT1_i023, POT1_i013, POT1_i015, POT1_i016, POT1_i021, POT1_i017, POT1_i019, POT3-1 and POT1_i024, respectively, all from the Dashuitang Formation; W–Y, Z–BB, CC–EE, FF–GG, HH, DDD, catalog nos. are POT4_i030, POT5_i047, POT8_i038, POT8_i040, POT10_i081 and POT14-1, respectively, all from the Nanshuba Formation; II–JJ, early juvenile specimen. (**KK–LL**, **MM–OO**) *Pavigondolella*? *vrielyncki* Kozur and Mock, 1991, catalog nos. are POT13_i061 (from the Nanshuba Formation) and POT1_i059 (from the Dashuitang Formation), respectively. (**PP–QQ, VV–AAA**) transitional form between *M. bidentata* and *P. andrusovi*; PP–QQ, POT11_i082, from the Nanshuba Formation; VV–XX, YY, ZZ**–**AAA, may be juvenile P_1 elements, catalog nos. are POT1_i010, POT1_i103 and POT8_i089, respectively; VV–YY, from the Dashuitang Formation; ZZ**–**AAA, from the Nanshuba Formation. (**RR–SS**) *Parvigondolella.* sp., POT12_i054, from the Nanshuba Formation. (**TT–UU**) *Parvigondolella andrusovi* Kozur and Mock, 1972, POT13_i057, from the Nanshuba Formation. **(BBB–CCC)** ?transitional form between *M. bidentata* and *Mi. hernsteini*, MDP25-1, from the Nanshuba Formation of the Madoupo section. A–AAA, from the Potou section. White arrows show the evolutionary trend from *M. bidentata* to *P. andrusovi*.

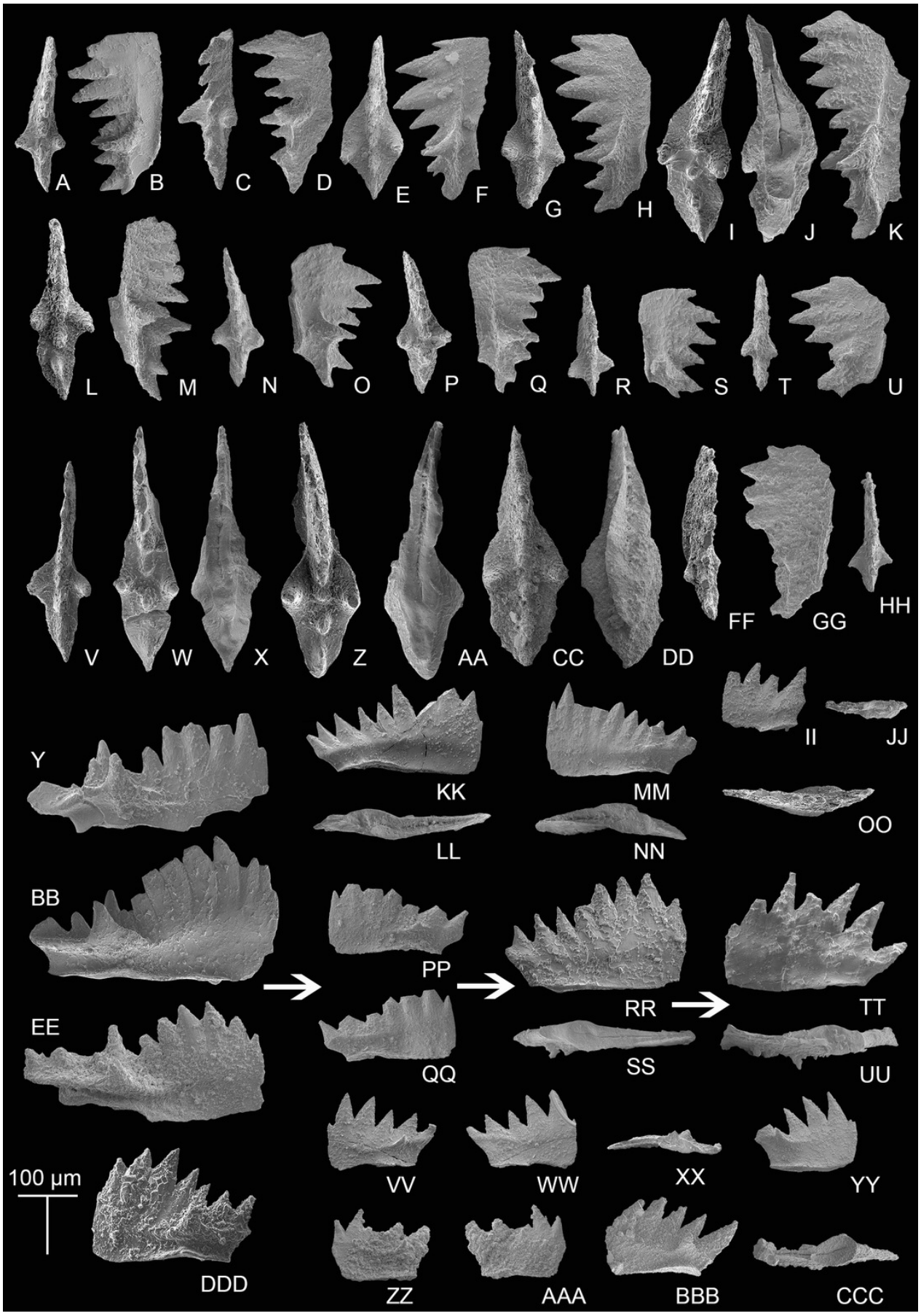
A
B
C
D
E
F
G
H
I
J
K
L
M
N
O
P
Q
R
S
T
U
V
W
X
Z
AA
CC
DD
FF
GG
HH
II
JJ
Y
KK
MM
OO
LL
NN
BB
PP
RR
TT
EE
QQ
SS
UU
100 µm
VV
WW
XX
YY
DDD
ZZ
AAA
BBB
CCC

Figure 7

SEM images of conodonts from the Nanshuba Formation of the Madoupo section.

(**A–O, DD**) *Mockina zapfei* (Kozur, 1973); A–C, D–F, G–I, J–L, M–O, DD, catalog nos. are MDP8_i040, MDP8_i061, MDP8_i109, MDP8_i039, MDP8_i043 and MDP10-4402, respectively. (**P–T**) *Mockina* sp. A; P–R, MDP8-031; S, MDP8-003; T, MDP8-032. (**U–CC**) *Mockina bidentata* (Mosher, 1968); U–V, W–X, Y–Z, AA, BB, CC, catalog nos. are MDP8_i044, MDP7_i115, MDP7_i116, MDP10-4503, MDP10-5207 and MDP7-3203, respectively. **(EE–FF)** ?*Mockina medionorica* Kozur, 2003, MDP8-011.

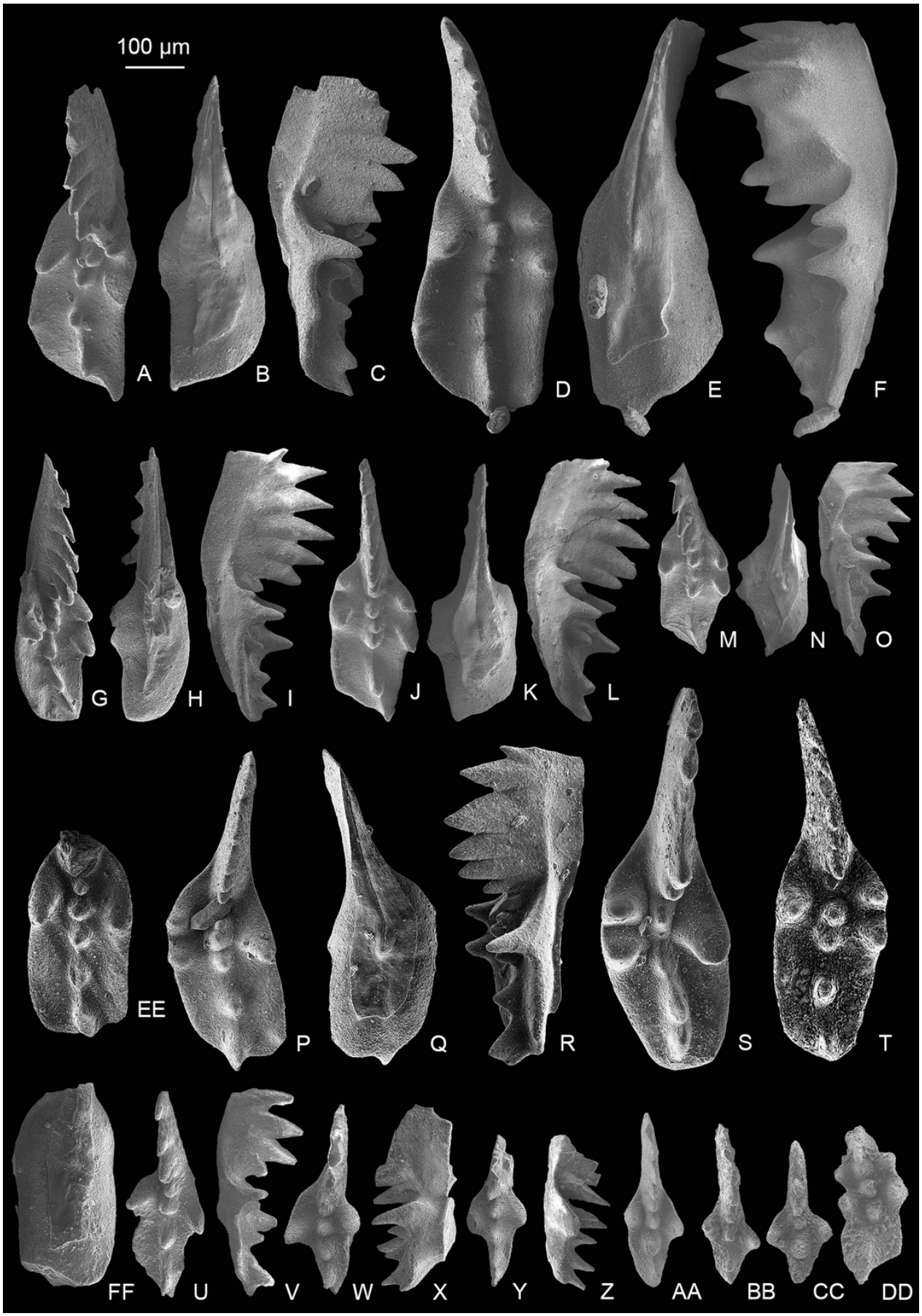
100 µm
A
B
C
D
E
F
G
H
I
J
K
L
M
N
O
EE
P
Q
R
S
T
FF
U
V
W
X
Y
Z
AA
BB
CC
DD

Figure 8

SEM images of *Mockina zapfei* (Kozur, 1973) from the Nanshuba Formation (Sevatian) of the Madoupo section in Baoshan, western Yunnan, China and its ontogenetic series.

(**A–T**) ontogenetic series; A, B, early juvenile species, catalog nos. are MDP8_1802 and MDP8-1901, respectively; C–E, F–H, late juvenile specimens, catalog nos. are MDP8-019 and MDP8_i108, respectively; I–K, early adult species, MDP8-902; L–N, adult species, MDP8_i035; O–Q, R–T, late adult species, catalog nos. are MDP8_i057 and MDP8_i055, respectively. (**U–Y**) the platform end of the P_1 element develops no terminal denticle; U–W, adult species, MDP_i037; X–Y, late juvenile species, MDP8-2909. (**Z–EE**) the P_1 elements develop small or tiny nodes on the platform end and one of the posterior lateral platform margins; Z–BB, CC–EE, catalog nos. are MDP8_i054 and MDP8-005, respectively.


A
B
C
D
E
F
G
H
I
J
K
L
M
N
O
P
Q
100 µm
R
S
T
U
V
W
X
Z
AA
BB
CC
DD
EE
Y

Figure 9

SEM images of *Mockina zapfei* (Kozur, 1973) from the Nanshuba Formation (Sevatian) of the Madoupo section in Baoshan, western Yunnan, China and its ontogenetic series.

(**A–N**) ontogenetic series; A, juvenile species, catalog no. is MDP7-4101; B, late juvenile species, MDP8-008; C**–**E, F**–**H, I**–**J, K, L**–**N, adult specimens, catalog nos. are MDP8-1301, MDP8-007, MDP8-801, MDP8-020 and MDP8-028, respectively. (**O–Q**) the P_1 element only has one pair of anterior marginal denticles, MDP8-022. (**R–Y**) simple ontogenetic series; R-S, juvenile species, MDP8_i052; T–V, W–Y, adult species, catalog no. is MDP8_i050 and MDP8_i046, respectively. Z–BB, variant species, MDP8_i038.

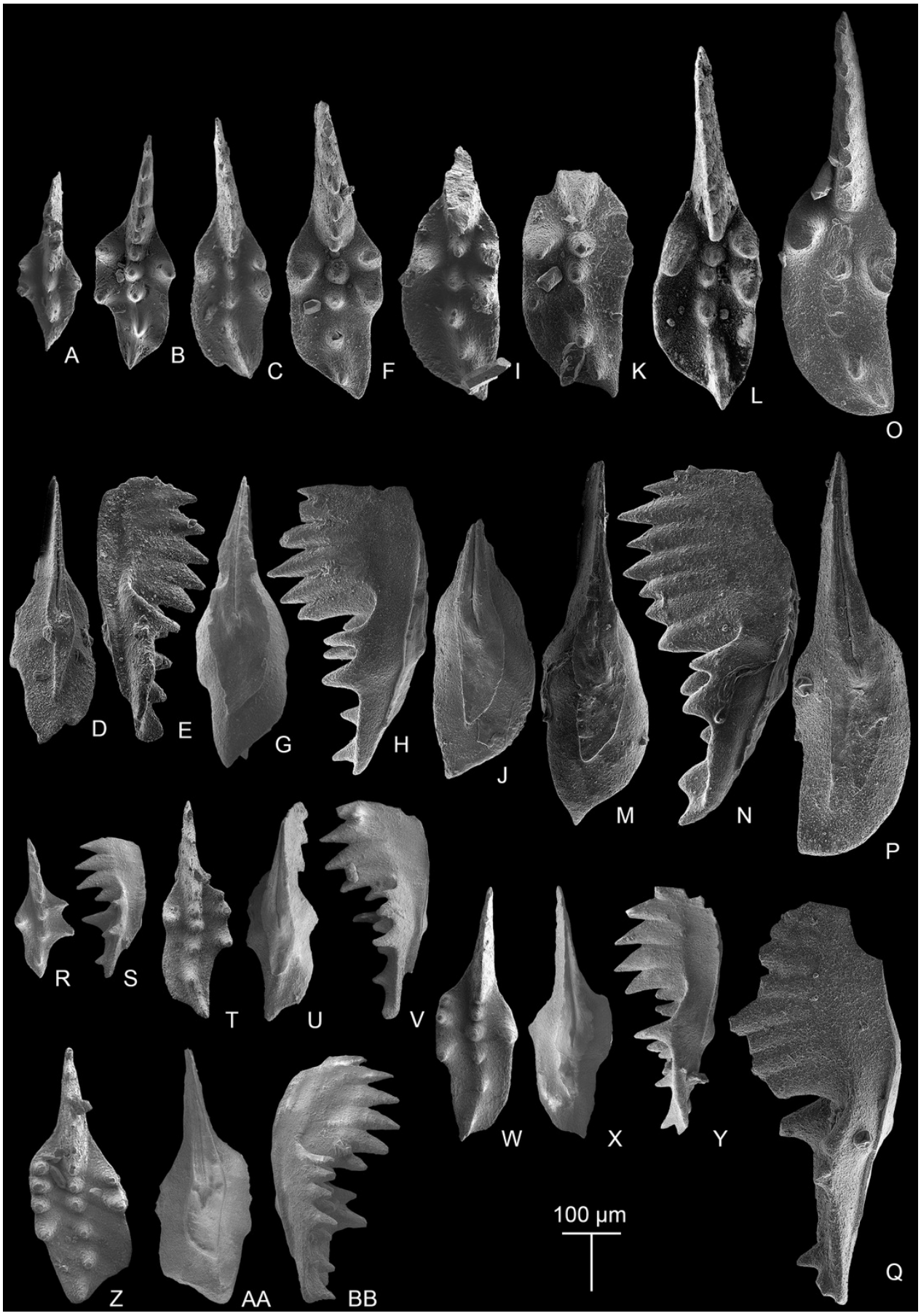
A
B
C
F
I
K
L
O
D
E
G
H
J
M
N
P
R
S
T
U
V
W
X
Y
Z
AA
BB
100 µm
Q

Table 1(on next page)

Reported conodont zonation of the Norian stage in China and its global correlation.

E. = Epigondolella, *M. = Mockina*, *P. = Parvigondolella*, *Mi. = Misikella*, *Me. = Metapolygnathus*, *C. =Carnepigondolella*, *tri. = triangularis*, *multi. = multidentata*, *posthern. = posthernsteini*, *G. = Guembelites*, *Ma. = Malayites*, *J. = Juvavites*, *Cy. = Cyrtopleurites*, *Hi. = Himavatites*, *Ha. = Halorites*, *S. = Sagenites*, *St. = Stikinoceras*, *D. = Drepanites*, *Mes. = Mesohimavatites*, *Gn. = Gnomohalorites*.

Table 1 Reported conodont zonation of the Norian stage in China and its global correlation

Substage	Wang and Wang, 1976 Tingri, Tibet	Qiu, 1984 Lhasa, Tibet	Tian, 1982 Nyalam, Tibet	Mao and Tian, 1987 Lhasa, Tibet	Wang and Wang, 1990, Yushu, Qinghai	Wang, 1993 Changdu, Tibet; Yidun, Sichuan	Yi et al., 2003 Qiangtang, Tibet	Ji et al., 2003 Lhasa, Tibet	Wang et al., 1986 Nada Hadan, Heilongjiang	Wang and Dong, 1985 Baoshan, Yunnan	Jin et al., 2022 Baoshan, Yunnan	This study Baoshan, Yunnan	Wang and Dong, 2006 Yunnan	Wang and Wang, 2016 China	Rigo et al., 2018 Tehtys		Orchard et al., 2007a, 2018, North America	
															Conodont Zones	Ammonoid Zones	Conodont Zones	Ammonoid Zones
□		□	□	□	□	□	□	□	□	□	□	□	*Mi. posthern.*	*Mi. hernsteini*	*Mi. posthern.*	□	*mosheri*	□
Sevatian	*E. abneptis*	*E. abneptis*	*E. abneptis*	*E. bidentata*	□	□	*E. bidentata -E.* sp.	unclear	*P. androsovi*	*E. bidentata*	□	*P. androsovi*	*Mi. hernsteini -P. androsovi*	*P. androsovi*	*Mi. hernsteini*	*S. quique-punctatus*	*bidentata*	*Gn. cordilleranus*
								E. bidentata	*E. bidentata*		*M. bidentata*	*M. bidentata* □	*E. bidentata*	*E. bidentata*	*P. androsovi* *M. bidentata*			
Alaunian								unclear			*M. slovakensis*				*M. slovakensis*	*Ha. macer*	*serrulata*	*Mes. columbianus*
				E. postera	*E. postera-abneptis abneptis-abneptis spatulatus*	*E. postera-E. abneptis*	*E. postera -abneptis spatulatus*	*E. postera*	*E. postera*	*E. postera*			*E. postera*	*E. postera*	*M. serrulata* *M. postera*	*Hi. hogarti*	*postera*	
				E. sp. C				*E. tozeri*							*M. spiculata*		*elongata*	
								E. spiculata									*spiculata*	
Lacian			*E. multi.*	*E. multi.*				unclear	*E. multi.*		□	□	*E. multi.*	*E. multi.*	*E. rigo-E.quadrata*	*Cy. bicrenatus*	*tozeri* *multi.*	*D. rutherfordi*
								?*E. tri.*	*E. abneptis*				*E. abneptis*	*E. abneptis*		*J. magnus*	*transformis*	?
																	triangularis	*J. magnus*
								unclear					*E. pseudodiebeli -E. abneptis*			*Ma. paulckei*	*quadrata*	*Ma. dawsoni*
								?*E. primitia*							*C. gulloae* *Me. parvus*	*G. jandianus*	*primitia*	*St. kerri*

Note: *E.* = *Epigondolella*, *M.* = *Mockina*, *P.* = *Parvigondolella*, *Mi.* = *Misikella*, *Me.* = *Metapolygnathus*, *C.* =*Carnepigondolella*, *tri.* = *triangularis*, *multi.* = *multidentata*, *posthern.* = *posthernsteini*, *G.* = *Guembelites*, *Ma.* = *Malayites*, *J.* = *Juvavites*, *Cy.* = *Cyrtopleurites*, *Hi.* = *Himavatites*, *Ha.* = *Halorites*, *S.* = *Sagenites*, *St.* = *Stikinoceras*, *D.* = *Drepanites*, *Mes.* = *Mesohimavatites*, *Gn.* = *Gnomohalorites*.

Table 2(on next page)

Stratigraphic distribution and statistic results of conodont species from the Potou section and the Madoupo section.

A. = *Ancyrogondolella*, *E.*= *Epigondolella*, *M.*= *Mockina*, *N*.= *Norigondolella, P*.= *Parvigondolella, Z*.= *Zieglericonus, Mi*. = *Misikella*. POT= Potou section, MDP= Madoupo section.

1 Table 2 Stratigraphic distribution and statistic results of conodont species from the Potou and the Madoupo sections.

Sample No.	?*A. praeslovakensis*	*E. carinata*	*E.* aff. *englandi*	*E. passerii*	*E.* sp.	*M. bidentata*	*M. elongata*	*M. medionorica*	?*M. medionorica*	*M. zapfei*	*Mockina* sp. A	transitional form between *M. bidentata*/*P. andrusovi*	?transitional form between *M. bidentata*/*Mi. hernsteini*	*M.* sp.	*P. andrusovi*	*P.* sp.	*P.? vrielyncki*	*N.?* sp. indet.	*Z.?* sp.	unidentifiable P_1 elements	S elements
POT14						1														1	
POT13															1		1				
POT12																1				1	3
POT11												1								1	
POT10						1														1	4
POT9					1	1														4	
POT8			1			2						1								3	
POT7				1																2	1
POT6														1				1	1	4	
POT5				1		2															
POT4						1															
POT3						1														1	
POT2				1										3							
POT1		2	5	3	2	11						3					1				
MDP26																					
MDP25													1								
MDP24																					
MDP23																					
MDP22																					
MDP21																					
MDP20																					
MDP19																					
MDP18																					
MDP17																					
MDP16																					
MDP15																					
MDP14																					
MDP13																					
MDP12								1													
MDP11																					
MDP10		2	1			3				1										4	
MDP9																				4	
MDP8	1	2			1	2	28	1	1	59	3									77	25
MDP7		5	2	4		6													1	15	3
MDP6																					
MDP5																					
MDP4																					
MDP3																					
MDP2																				1	
MDP1																					

2

Table 3(on next page)

Reported conodont form species in the *Mockina bidentata* Zone.

Table 3 Reported conodont form species in the *M. bidentata* Zone

E. abneptis	Huckriede (1958), Mosher (1968), Krystyn (1980), Wang & Dong (1985)
E. englandi	Orchard (1991b), Orchard et al.(2007b), Krystyn et al. (2007), Onoue et al. (2018); Wang et al. (2019), Du et al. (2020), Karádi et al. (2021)
E. aff. *englandi*	Wang et al. (2019, figs. 6.2–6.3), This study
E. carinata	Orchard (1991b), Carter & Orchard (2007), Orchard et al.(2007b), Du et al.(2020), this study
E. passerii	Krystyn (1980, pl. 13, fig. 17–18), Jin et al. (2022), this study
E. spiculata	Yamashita et al. (2018)
M. elongata	Yamashita et al. (2018), Jin et al. (2022, fig. 4.8), this study
M. longidentata	Kovács & Kozur (1980)
M. mosheri	Kovács & Kozur (1980), Krystyn et al. (2007), Yamashita et al. (2018), Du et al. (2020), Karádi et al. (2021), Jin et al. (2022)
M. medionorica	Kovács & Kozur (1980, pl. 4, fig. 5), this study
M. postera	Kozur & Mostler (1972), Kovács & Kozur (1980), Krystyn (1980), Wang & Wang (1985), Gullo (1996), Channell et al. (2003), Muttoni et al. (2004), Dong & Wang (2006), Rožič et al. (2009)
M. sakurae	Zeng et al. (2021)
M. slovakensis	Gullo, 1996; Giordano t al., 2010; Muttoni et al., 2004; Dong & Wang (2006), Rigo et al., 2018; Yamashita et al. (2018) Du et al., 2021; Jin et al., 2022
M. cf. *slovakensis*	Channell et al. (2003)
M. zapfei	Channell et al. (2003), Hornung (2005), Giordano t al. (2010), Rigo et al. (2018), Du et al. (2021), this study
M. cf. *zapfei*	Bazzucchi et al. (2005), Rigo et al. (2016)
N. steinbergensis	Mosher (1968), Kovács & Kozur (1980), Krystyn (1980), Orchard (1991b), Channell et al. (2003), Hornung (2005), Orchard et al. (2007b), Rožič et al. (2009), Mazza et al. (2012), Onoue et al. (2018), Du et al. (2020)
P.? *vrielyncki*	Channell et al. (2003), Rigo et al. (2018); Du et al. (2021), this study
P. aff. *vrielyncki*.	Yamashita et al. (2018)
P. lata	Du et al. (2021)
P_1 elements of *Parvigondolella*	Orchard et al.(2007b), Orchard (1991b), e.g.
conical P_1 elements	Channell et al., 2003; Du et al., 2021, this stuy
Transitional forms from *M. bidentata*	Karádi et al. (2020), Du et al. (2021), Zeng et al. (2021), this study
M. carinata? in Du et al. (2020), *E. triangularis*? in Channell et al. (2003), *O.*? *multidentata* in Kovács & Kozur (1980), *M.* aff. *tozeri* and *E. uniformis*? in Onoue et al. (2018), other indeterminated P_1 elements.	